Monthly Notices
of the
ROYAL ASTRONOMICAL SOCIETY

Mon. Not. R. Astron. Soc. **410,** 2428–2445 (2011) doi:10.1111/j.1365-2966.2010.17619.x

Discovery of 59 ms pulsations from 1RXS J141256.0+792204 (Calvera)

S. Zane,[1⋆] F. Haberl,[2] G. L. Israel,[3] A. Pellizzoni,[4] M. Burgay,[4] R. P. Mignani,[1] R. Turolla,[1,5] A. Possenti,[4] P. Esposito,[4,6] D. Champion,[7] R. P. Eatough,[7] E. Barr[7] and M. Kramer[7]

[1]*Mullard Space Science Laboratory, University College London, Holmbury St Mary, Dorking, Surrey RH5 6NT*
[2]*Max-Planck-Institut für extraterrestrische Physik, Giessenbachstrasse, D-85748, Garching, Germany*
[3]*INAF-Osservatorio Astronomico di Roma, via Frascati 33, I-00040 Monteporzio Catone, Italy*
[4]*INAF-Osservatorio Astronomico di Cagliari, località Poggio dei Pini, strada 54, I-09012 Capoterra, Italy*
[5]*Department of Physics, University of Padova, via Marzolo 8, 35131 Padova, Italy*
[6]*INFN – Istituto Nazionale di Fisica Nucleare, sezione di Pavia, via A. Bassi 6, I-27100 Pavia, Italy*
[7]*Max-Planck-Institut für Radioastronomie, Auf dem Hügel 69, 53121 Bonn, Germany*

Accepted 2010 August 28. Received 2010 August 19; in original form 2010 July 7

ABSTRACT

We report on the results of a multi-wavelength study of the compact object candidate 1RXS J141256.0+792204 (Calvera). Calvera was observed in the X-rays with *XMM–Newton*/EPIC twice for a total exposure time of ∼50 ks. The source spectrum is thermal and well reproduced by a two-component model composed of either two (absorbed) hydrogen atmosphere models or two blackbodies with temperatures $kT_1 \sim 55/150$ eV, $kT_2 \sim 80/250$ eV, respectively (as measured at infinity). Evidence was found for an absorption feature at ∼0.65 keV while no power-law high-energy tail is statistically required. Using pn and MOS data we discovered pulsations in the X-ray emission at a period $P = 59.2$ ms. The detection is highly significant ($\gtrsim 11\sigma$), and unambiguously confirms the neutron star nature of Calvera. The pulse profile is nearly sinusoidal, with a pulsed fraction of ∼18 per cent. We looked for the timing signature of Calvera in the *Fermi* Large Area Telescope (LAT) data base and found a significant ($\sim 5\sigma$) pulsed signal at a period coincident with the X-ray value. The gamma-ray timing analysis yielded a tight upper limit on the period derivative, $\dot{P} < 5 \times 10^{-18}$ s s^{-1} ($\dot{E}_{\rm rot} < 10^{33}$ erg s^{-1}, $B < 5 \times 10^{10}$ G for magneto-dipolar spin-down). Radio searches at 1.36 GHz with the 100-m Effelsberg radio telescope yielded negative results, with a deep upper limit on the pulsed flux of 0.05 mJy. Diffuse, soft (<1 keV) X-ray emission about 13 arcmin west of the Calvera position is present both in our pointed observations and in archive *ROSAT* all-sky survey images, but is unlikely associated with the X-ray pulsar. Its spectrum is compatible with an old supernova remnant (SNR); no evidence for diffuse emission in the radio and optical bands was found. The most likely interpretations are that Calvera is either a central compact object escaped from a SNR or a mildly recycled pulsar; in both cases the source would be the first ever member of the class detected at gamma-ray energies.

Key words: stars: neutron – pulsars: general – pulsars: individual: 1RXS J141256.0+792204 (Calvera) – gamma-rays: stars – X-rays: stars.

1 INTRODUCTION

Isolated neutron stars (NSs) have been for a long time associated with radio pulsars. It was only during the last two decades, thanks to multi-wavelength observations from both space- and ground-based instruments, that our picture of the Galactic NS population changed. These observations unveiled the existence of different types of isolated NSs which are radio quiet or have radio properties quite at variance with those of ordinary pulsars. Examples are the soft gamma repeaters and the anomalous X-ray pulsars (the likely magnetars; e.g. Woods & Thompson 2006; Mereghetti 2008), the central compact objects (CCOs; e.g. Pavlov, Sanwal & Teter 2004; De Luca 2008) in supernova remnants (SNR), the seven dim *ROSAT* sources [X-ray Dim Isolated NSs (XDINSs); e.g. Haberl (2007); Turolla (2009)] and the more recently discovered rotating radio transients (RRATs; McLaughlin et al. 2006). Observations at X-ray,

⋆E-mail: sz@mssl.ucl.ac.uk

gamma-ray and optical wavelengths have been crucial in revealing the rich variety of NS properties and their phenomenology.

Only a limited number ($\leq$20; in comparison with $\sim$2000 known ordinary radio pulsars) of sources in each of these new isolated NS classes has been identified so far. This makes establishing links between different groups hazardous and no unitary picture of the Galactic NSs has emerged to date. The search for new members of each class is therefore of the utmost importance, as is the study of objects with properties intermediate between those of known groups which could provide the much needed missing links.

In this respect, it appears very promising that two new, apparently radio-quiet, X-ray sources have been recently proposed as isolated NS candidates. These are 1RXS J141256.0+792204 (dubbed Calvera; Hessels et al. 2007; Rutledge, Fox & Shevchuk 2008; Shevchuk, Fox & Rutledge 2009), which was found in the *ROSAT* Bright Source Catalogue (RBSC; Voges et al. 1999), and, at fainter flux levels, 2XMM J104608.7−594306, discovered with *XMM–Newton* (Pires et al. 2009).

Calvera, in particular, is a puzzling source and its interpretation represented a conundrum (see Section 2). At variance with most known radio-quiet isolated NSs, the source is at high Galactic latitude, and it exhibits a quite hot, thermal spectrum with little absorption. Calvera was first selected in the RBSC and identified as a possible isolated NS candidate on the basis of its large X-ray-to-optical flux ratio. The source was then observed with the *Swift*-X-ray Telescope (XRT) and with *Chandra* (see Section 2 for details of the past observations, and references therein). In particular, the first, short ($\sim$2 ks) *Chandra* pointing (obs. ID: 8508) provided a refined X-ray position and follow-up *Gemini* observations confirmed the lack of optical counterparts down to $g \sim 26.3$, implying $F_{\rm X}/F_{\rm opt} > 9000$ (Rutledge et al. 2008). However, despite the improved spectral information, these data were insufficient to discriminate among the different interpretations for its nature.

Clearly, better spectral and timing information is crucial to unambiguously classify the source. Here, we present a multi-wavelength study of Calvera, based on two new *XMM–Newton* observations, on the analysis of publicly available *Fermi*-Large Area Telescope (LAT) data, and on a new radio observation taken at the 100-m Effelsberg telescope. We also used *Chandra* and *ROSAT* archival data. The paper is organized as follows. We first summarize the results from the past observations and the proposed scenarios in Section 2. Spectral and timing results from the *XMM–Newton* and *Fermi*-LAT observations are presented in Section 3, while the radio observations are summarized in Section 4. A search for potential sources of diffuse X-ray or radio emission in the proximity of Calvera is presented in Section 5, and discussion and conclusions follow in Sections 6 and 7.

2 PAST OBSERVATIONS AND PROPOSED SCENARIOS

The first X-ray observations of Calvera, taken with the *Swift*-XRT, had very limited counting statistics (74 source counts in the 0.3–10 keV range) and only allowed a very preliminary spectral analysis (Rutledge et al. 2008): the spectrum appeared rather hard, but the spectral model was virtually unconstrained. A blackbody (BB) fit gave temperature $kT_{\rm BB} \sim 215$ eV, radius $R_{\rm BB} \sim 7$ km (for a 10 kpc distance), while a power-law (PL) model yielded a photon index $\Gamma \sim 2.8$. The 0.3–10 keV flux was 1.2×10^{-12} and 2.5×10^{-13} erg cm^{-2} s^{-1} for the two models, respectively. A thermal bremsstrahlung and a Raymond–Smith plasma model were also tried, providing temperatures of $\sim$0.8 and $\sim$1.5 keV. No estimate of the interstellar absorption was derived (in all fits $N_{\rm H}$ was held fixed to the total Galactic value obtained from Kalberla et al. 2005), so the source distance was unconstrained.

On the basis of the very limited spectral information obtained with the *Swift* data, Rutledge et al. (2008) discussed several intriguing possibilities for the nature of Calvera. However, they also concluded that none of them was without problems. For instance, they proposed that the source may be an XDINS, but hotter than the other members of the class ($kT_{\rm BB} \sim$ 40–100 eV). In this case, under the arbitrary assumption that the emitting radius is the same for all objects of the class, the observed flux would imply a distance of $\sim$2–8 kpc from the Sun and a height of $\sim$1.3–5.1 kpc above the Galactic plane. Taken at face value, this appears hardly compatible with the star's age as derived from its temperature (assuming standard cooling models), unless either Calvera has an unprecedented high velocity (a few thousand km s^{-1}), or did not cool according to conventional models, or it has been re-heated by some unknown mechanisms.

A magnetar identification was also recognized to be problematic. For an average quiescent magnetar luminosity of $\approx 10^{35}$ erg s^{-1}, the flux inferred from the best fit of the *Swift*-XRT spectrum would imply a distance of at least 66 kpc, and a height of 40 kpc above the Galactic plane. Calvera would then be the first magnetar to belong to a halo population. Although evidence of massive compact object formation in the halo has been found (e.g. Mirabel et al. 2001), this interpretation was considered statistically unlikely. On the other hand, a Galactic plane population origin would require a luminosity fainter by about 5 orders of magnitude, in which case Calvera would be a candidate for the faintest, and maybe the oldest, identified magnetar.

Rutledge et al. (2008) also considered the idea that Calvera might be a CCO. In this case, assuming an average NS velocity of $\approx$400 km s^{-1} and a cooling age of 0.5 Myr (Page et al. 2004), the present location of Calvera would imply a distance of $\sim$300 pc which would make it a factor of $\approx$10 fainter than other known CCOs.

The last alternative proposed by Rutledge et al. (2008) was an old millisecond pulsar. This scenario would place the source at a distance of a few hundred pc, the exact value depending on the assumed size of the hot polar caps. Interestingly, for such a small distance, the derived upper limit in the optical of $g > 26.3$ reported by Rutledge et al. (2008) is deep enough to rule out both a white and a red dwarf companion. If this is the case, Calvera would thus be one of the few solitary field millisecond pulsars discovered so far (about 18 known isolated millisecond pulsars in the Galactic plane, comprising roughly 30 per cent of the population).

In order to shed further light on these possibilities, Shevchuk et al. (2009) re-observed the source with *Chandra* for 30 ks on 2008 April 8 (obs. ID: 9141). This longer observation allowed them to exclude (absorbed) single-component spectral models, as a BB, a PL or a pure hydrogen atmospheric model (NSA; Zavlin, Pavlov & Shibanov 1996), since they all gave unacceptably large values of χ^2 and, in some cases, a value of the column density larger than the Galactic one in the source direction ($N_{\rm gal} = 2.65 \times 10^{20}$ cm^2; Kalberla et al. 2005). Instead, these authors proposed as best fit a NSA model (with effective temperature of $\approx$110–120 eV) combined with a spectral feature, either an edge or more likely an emission line, at $\sim$0.5–0.6 keV. The source did not show signs of variability either on short or long (>1 year) time-scales, and pulsations have not been detected down to a 3σ limit of 20–30 per cent in pulsed fraction (defined as the semi-amplitude of the sinusoidal modulation divided by the mean source count rate) in the period range between 0.9 s and 10^4 s. The absence of a non-thermal spectral component

and the relatively low limit on the pulsed fraction for periods of a few seconds made a magnetar interpretation unlikely, but the other possibilities still remained open. Therefore, despite the better spectrum, the *Chandra* data (obs. ID: 9141) did not provide sufficient clues to solve the conundrum proposed by Rutledge et al. (2008) about the nature of the source.

3 X-RAY AND GAMMA-RAY OBSERVATIONS

3.1 Source position and association

We started our analysis by first accurately re-assessing the source position determination. This is particularly important because a large positional error precludes firmly ruling out the association with the close-by ($\sim$0.9 arcsec) $g \sim 24.8$ Star A (Rutledge et al. 2008).

Based on a *Chandra*/HRC-I observation (obs. ID: 8508), Rutledge et al. (2008) gave: $\alpha = 14^{\rm h}12^{\rm m}55\overset{\rm s}{.}885$, $\delta = +79^\circ22'04\overset{''}{.}10$, with a 90 per cent uncertainty of 0.57 arcsec, after applying a bore sight correction of $\Delta\alpha = -0.04 \pm 0.22$ arcsec and $\Delta\delta = +0.95 \pm 0.22$ arcsec to the *Chandra* astrometry.[1] To this aim, they used as a reference the optical coordinates of a second source, CXOU J141259.43+791958, detected in the HRC-I field, derived from those of its putative counterpart identified in their *Gemini* images, calibrated with the USNO-B1.0 catalogue (Monet et al. 2003). However, this procedure comes with some caveats.

To verify the value of the Rutledge et al. (2008) coordinates, we retrieved the HRC-I data set (obs. ID: 8508) from the public *Chandra* archive. First of all, we found that their reference X-ray source has a count rate of $\approx$0.005 count s^{-1} ($\approx 2.5\sigma$ detection significance), which lowers the accuracy of the bore sight correction. Furthermore, using only one reference source can introduce systematics due to a proper motion of its putative optical counterpart. Since the default reference epoch for the USNO-B1.0 coordinates is 2000.0[2] while the epoch of the *Chandra*/HRC-I observation (obs. ID: 8508) is 2007.13, the effect on the bore sight correction can be significant. We identified the putative counterpart of the reference X-ray source with the USNO-B1.0 star 1693−0051235 ($B = 20.51$; $R = 19.4$). According to the catalogue, this star has a proper motion $\mu_\alpha = -6 \pm 4$ mas yr^{-1} and $\mu_\delta = 6 \pm 1$ mas yr^{-1}, with ± 4 mas yr^{-1} being a more realistic uncertainty for the latter value (see e.g. Gould 2003). This would imply an offset of $\Delta\alpha \sim +42 \pm 28$ mas and $\Delta\delta = -42 \pm 28$ mas in the bore sight correction, apparently not accounted for in Rutledge et al. (2008). While this offset would be negligible within the error budget of the *Chandra* and of the USNO-B1.0-based astrometry calibration of the *Gemini* images (Rutledge et al. 2008), we cannot rule out that the star has a larger proper motion. We queried other astrometric catalogues to verify the USNO-B1.0 proper motion. Unfortunately, the star is too faint to be in the UCAC-3 catalogue (Zacharias et al. 2010) while it appears in the PPMXL (Roeser, Demleitner & Schilbach 2010) which gives $\mu_\alpha = -7.1 \pm 5.6$ mas yr^{-1} and $\mu_\delta = 6.1 \pm 5.6$ mas yr^{-1}, consistent with the USNO-B1.0 value although not statistically significant yet. From this value, we set a 3σ upper limit on the star proper motion of $\mu_\alpha = 24$ mas yr^{-1} and $\mu_\delta = 23$ mas yr^{-1}. Thus, we estimate an additional uncertainty of $\sim$0.17 arcsec (per coordinate) to the one-star bore sight correction of Rutledge et al. (2008), rising its total uncertainty to 0.28 arcsec (per coordinate).

We independently measured the coordinates of Calvera in the HRC-I data set, after it was corrected for the reported offset in the absolute *Chandra* astrometry. Our best-fitting coordinates are then $\alpha = 14^{\rm h}12^{\rm m}55\overset{\rm s}{.}64$, $\delta = +79^\circ22'03\overset{''}{.}7$, with a 90 per cent confidence error of 0.6 arcsec. Given the re-assessed uncertainty on the one-star bore sight correction (see above), we decided not to apply it to the measured coordinates of Calvera.

A second *Chandra* observation of Calvera was performed with the ACIS-S detector (Shevchuk et al. 2009, obs. ID: 9141). We retrieved the ACIS-S data set from the public *Chandra* archive, and we measured the position of Calvera as $\alpha = 14^{\rm h}12^{\rm m}55\overset{\rm s}{.}84$, $\delta = +79^\circ22'03\overset{''}{.}7$, with a 90 per cent confidence error of 0.6 arcsec. This position is consistent with that measured by us using the HRC-I data set and, obviously, virtually identical to that obtained by Shevchuk et al. (2009) from the uncorrected *Chandra* astrometry. We noticed that Shevchuk et al. (2009) applied the bore sight correction of the ACIS-S image, using the position of the optical counterparts to two field sources, CXOU J141220.78+792251.6 and CXOU J141246.23+792222.3. They then obtained $\alpha = 14^{\rm h}12^{\rm m}55\overset{\rm s}{.}76$, $\delta = +79^\circ22'03\overset{''}{.}4$ with a quoted 90 per cent uncertainty of 0.31 and 0.3 arcsec in right ascension and declination, respectively. However, we could not detect these two sources in the ACIS-S (above a detection threshold of 3σ; see Fig. 1, left panel). We confirm, instead, the marginal detection of a faint source, CXOU J141252.41+792152.60, in the ACIS-S data located $\sim$20 arcsec south west of Calvera, which was not detected in the HRC-I data (obs. ID: 8508), while the HRC-I source CXOU J141259.43+791958 falls out of the ACIS-S field of view. Because of the non-detection of the two sources claimed by Shevchuk et al. (2009) in the ACIS-S data, we used the nominal *Chandra* position in the present analysis.

Finally, for the sake of completeness we checked our *XMM–Newton* observations. *XMM–Newton* observed Calvera twice in 2009, on August 31 and October 10, for a total exposure of about 47 ks. The observations were performed with the EPIC pn (Strüder et al. 2001) and MOS (Turner et al. 2001) cameras in different CCD read out modes (see Table 1). The net exposure from the first observation (obs. ID: 0601180101) was short: less sources were detected and no bore sight correction was performed. From the second observation (obs. ID: 0601180201), we obtained $\alpha = 14^{\rm h}12^{\rm m}55\overset{\rm s}{.}48$, $\delta = +79^\circ22'03\overset{''}{.}3$, as computed by the EPIC pipeline (1σ statistical error of 0.21 arcsec) which computes the bore sight correction from the positions of X-ray sources in the field matched against those of optical sources in e.g. the USNO-B1.0, NASA/IPAC Extragalactic Database (NED) and Naval Observatory Merged Astrometric Dataset (NOMAD) catalogues. In this case, the pipeline finds 35 X-ray sources with optical matches. However, we visually inspected the X-ray source position on the DSS-2 images and we found possible matches with 14 optical sources, of which only four are listed both in the GSC-2 (Lasker et al. 2008) and in the 2MASS (Skrutskie et al. 2006) catalogues. By matching the pixel-to-sky coordinates of the X-ray sources and their associated 2MASS/GSC-2 counterparts, we derived an astrometric solution with an rms of 0.88 arcsec and we determined $\alpha = 14^{\rm h}12^{\rm m}55\overset{\rm s}{.}68$, $\delta = +79^\circ22'04\overset{''}{.}2$ for Calvera, formally more consistent with the coordinates obtained from the *Chandra* data sets.

[1] As the authors noted, this large correction was probably due to a systematic 0.4 arcsec offset in the absolute *Chandra* astrometry affecting data taken after 2006 December 1.

[2] USNO-B1.0 coordinates are extrapolated to epoch 2000.0 from the mean epoch of observations according to the proper motions computed by the USNO-B1.0 pipeline. However, the uncertainty due to the proper motion extrapolations is not accounted for in the nominal coordinate accuracy. This implies larger errors on any USNO-B1.0-based astrometric solution and on the coordinates thereby determined.

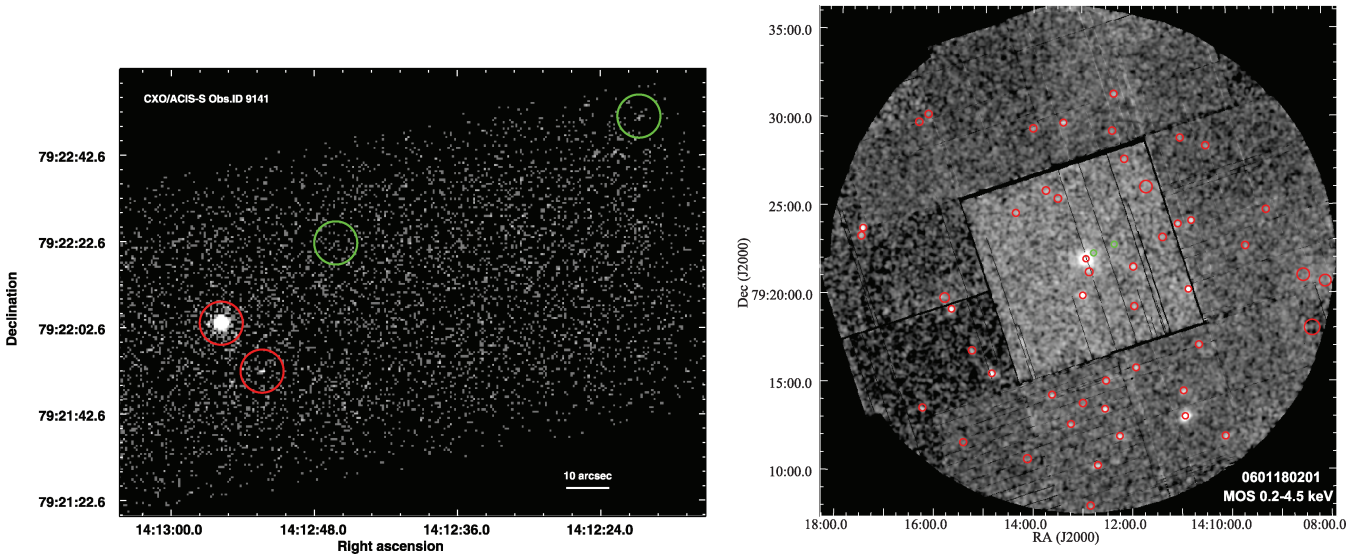

Figure 1. Left-hand panel: *Chandra* image of the field taken in 2008 (obs. ID: 9141). Red circles mark the two detected sources: Calvera ($\alpha = 14^{\rm h}12^{\rm m}55\overset{\rm s}{.}83$, $\delta = 79^\circ22'3\overset{''}{.}7$, uncertainty = 0.63 arcsec at 90 per cent confidence level, counts $s^{-1} = 0.180 \pm 0.003$) and CXOU J141252.41+792152.60 ($\alpha = 14^{\rm h}12^{\rm m}52\overset{\rm s}{.}41$, $\delta = 79^\circ21^{\rm m}52\overset{''}{.}6$, uncertainty = 1.41 arcsec at 90 per cent confidence level, count $s^{-1} = 0.00052 \pm 0.00018$). Note that these two sources are not resolved in the *XMM–Newton* data, but, given the low count rate of the second one, we do not expect a significant contamination in our spectral and timing analysis. The green circles mark the positions of the two sources used by Shevchuk et al. (2009) for the bore sight correction; note they are undetected in our analysis of the *Chandra* data. Right panel: combined EPIC MOS1/2 image in the 0.2–4.5 keV band, with the detected sources marked by red circles. MOS1 was in imaging mode, covering the target and the surrounding field (central CCD + 5 outer CCDs), while MOS2 was in timing mode (imaging for outer six CCDs). Green circles correspond to the green circles on the *Chandra* image.

Table 1. *XMM–Newton* EPIC observations of Calvera.

Observation ID	EPIC[a]	Start-end time (UT)	Exp.[b] (ks)
0601180101	pn SW	2009-08-31 07:14–15:09	14.0/13.94
	M1 FF	07:08–15:09	19.6/19.65
	M2 TU	07:08–15:05	20.0/ –
0601180201	pn SW	2009-10-10 04:15–12:27	14.5/19.48
	M1 FF	04:09–12:26	20.3/27.44
	M2 TU	04:09–12:22	20.4/ –

[a]Instrument configurations: pn SW: Small Window CCD readout mode with 6 ms frame time; MOS1 (M1) FF: Full Frame, 2.6 s; MOS2 (M2) TU: Timing Uncompressed, 1.75 ms; The thin optical blocking filter was used for all cameras.
[b]Net exposures used for timing and spectral analysis (dead-time corrected).

We notice that the two sources used by Shevchuk et al. (2009) for the *Chandra* bore sight are also not detected by *XMM–Newton* (see Fig. 1, right-hand panel). From the sensitivity map of observation 0601180201 (pipeline), the 3σ upper limit for the two sources is 0.005 count s^{-1} (in the EPIC total band 0.2–12 keV), a factor of 30 lower than the count rate of Calvera. This converts to a flux of $\approx 3 \times 10^{-14}$ erg cm^{-2} s^{-1}, with sizeable uncertainties depending on the assumed spectral model.

In conclusion, through our astrometry analysis we conclude that the most reliable coordinates of Calvera are those derived from the *Chandra* astrometry ($\alpha = 14^{\rm h}12^{\rm m}55\overset{\rm s}{.}84$, $\delta = +79^\circ22'03\overset{''}{.}7$, with a 90 per cent confidence error of 0.6 arcsec) i.e. without applying uncertain bore sight corrections, and they indeed confirm that Calvera is not associated with star A from Rutledge et al. (2008). Moreover, we note that the uncertainty on the Calvera coordinates is small enough not to hamper a sensitive search for coherent signals in our timing analyses (see Section 3.5).

3.2 *XMM–Newton* data analysis

For both, spectral and timing analysis, we used the latest *XMM–Newton* Science Analysis Software (SAS), version 10.0.1. We checked that the pn event files produced by 'epchain' were clean of unrecognized time jumps before we applied an event time randomization.

We extracted source spectra for Calvera from the imaging mode data of pn and MOS1 using a circular region around the target position with 15 arcsec radius and background spectra from a nearby source-free region of same size. Based on its low number of counts (see Fig. 1 and its caption), CXOU J141252.41+792152.60 is not expected to contaminate Calvera's data. Since the spectral response in MOS timing mode is currently not well calibrated, we did not use the MOS2 timing data for spectral analysis. For spectra we selected single pixel events (corresponding to PATTERN = 0) for pn and all valid events for MOS (PATTERN = 0–12), excluding bad CCD pixels and columns (FLAG = 0). We used XSPEC version 12.5.0 for spectral modelling.

The same pn and MOS event lists considered for the spectral analysis were also used as input for the timing analysis (with different background screening criteria; see Table 1). In addition, in order to obtain better temporal resolution, we also used the MOS2 data. MOS2 was operated in timing mode; in this mode data from the central CCD are collapsed into a one-dimensional row to achieve a ∼1.75 ms time resolution. Therefore, instead of a circular extraction region, we used a rectangular box of 20 pixel width. The local background was measured in a region of the images far from the extracted source itself and taking care that no other source falls within the extraction regions by chance (as we already noticed, the *Chandra* source CXOU J141252.41+792152.60 is unresolved from Calvera; see Section 3.1). The arrival times of the photons were corrected to the barycentre of the Solar system using the JPL

DE405 Solar system ephemeris (Standish 2004) and the SAS task 'BARYCEN'.

3.3 *XMM–Newton* spectral analysis: pulse averaged spectra

Spectra were accumulated from the pn and MOS1 event lists after removing those time intervals affected by solar proton flares resulting in an effective exposure time of ∼14 ks (pn) and ∼19.7 ks (MOS1; first observation, obs. ID: 0601180101), 19.5 ks (pn) and 27.5 ks (MOS1; second observation, obs. ID: 0601180201).

We started the analysis considering an absorbed double BB model and fitting the two pn and the two MOS1 spectra simultaneously, allowing only a renormalization factor to account for cross-calibration uncertainties between the detectors and possible time-variability of the source. To account for interstellar absorption, here and in the following we adopted the elemental abundances of Wilms, Allen & McCray (2000, model 'phabs' in XSPEC). We note here that the used metal abundances influence the derived equivalent hydrogen column density and can introduce systematic uncertainties when comparing its value with H I-derived column densities. We did not find flux variations greater than 3 per cent between the two observations, which is consistent, considering the statistical uncertainties, with a steady source flux. We then performed an independent fit of the spectra from the first and the second observation (still joining pn and MOS data within each epoch). The resulting best-fitting parameters, from the two epochs, were consistent within their statistical errors.

Since the source showed neither significant flux variations nor spectral changes between the two *XMM–Newton* observations, in the rest of the analysis we fitted all pn and MOS data together in order to obtain the best signal-to-noise ratio (S/N). We tested several single, double and triple component spectral models, based on different combinations of BBs, PLs, NS atmosphere models (NSA) and absorption edges or Gaussian lines. In the NSA model, we used $R_{\rm star} = 12$ km and $M_{\rm star} = 1.4\,{\rm M}_{\odot}$ as input parameters for the NS radius and mass. The results are summarized in Table 2, where we report only the fluxes inferred from the pn data of observation 0601180101. As mentioned above, we do not see significant flux variations between the two observations: computing an average pn flux for the two observations, weighted with the exposures, gives a value 0.98 times smaller than that reported in Table 2. Also, the fluxes obtained from the MOS1 spectra are consistent with those listed in the table. We warn the reader that the parameters reported in Table 2 have a different physical meaning in as much the best-fitting temperatures obtained by the BB fit are measured at infinity, while those from the NSA model are measured at the NS starface. The two quantities are related by $T_{\infty} = T/(1+z)$ where $1+z \equiv 1/\sqrt{1-2.952 M_{\rm star}/R_{\rm star}}$ is the gravitational redshift factor.

In agreement with Shevchuk et al. (2009), we find that single-component models do not provide a good representation of the Calvera spectrum. However, the advantage of the EPIC spectra is the higher efficiency of the instruments below 500 eV, where the *Chandra* spectrum has very few counts. Fitting the *XMM–Newton* data with one-component models leaves a low energy excess, that can be accounted for by a second emission component. Two-component models including a PL (as in the combinations PL+BB, PL+NSA) demonstrate a problem: the additional PL is always very steep and represents the soft part of the spectrum (requiring a high interstellar absorption), instead of a hard tail as usually seen from isolated NSs with a non-thermal component (De Luca et al. 2005). Instead, we found that the best two-component fits are composed of either, two thermal components (BB+BB, NSA+NSA) or a NSA+edge model. One difference is that, while the NSA+edge fit gives a value of $N_{\rm H}$ consistent with the Galactic one (as in the case of the *Chandra* data; Shevchuk et al. 2009), the fits with two thermal components

Table 2. Summary of spectral fits.

Model	χ^2_r/d.o.f.	$N_{\rm H}$ 10^{20} ($\rm cm^{-2}$)	Γ	kT^a (eV)	$E_{\rm edge}/E_{\rm line}$ (keV)	τ/σ	$\rm F^b_{obs}$ 10^{-13} ($\rm erg\,cm^{-2}\,s^{-1}$)	$\rm F_{bol}{}^c$ 10^{-12} ($\rm erg\,cm^{-2}\,s^{-1}$)	Comment
PL[d]	1.843/326	11.9	3.4				9.12	–	$N_{\rm H} > N^e_{\rm gal}$
PL + BB	1.055/324	8.9 ± 1.0	3.8 ± 0.3	227 ± 8			8.58	0.51	$N_{\rm H} > N_{\rm gal}$
PL + NSA	1.051/324	9.1 ± 0.8	4.3 ± 0.5	111 ± 7			8.49	1.28	$N_{\rm H} > {\rm N_{gal}}$
BB[d]	2.258/326	0.0		198			8.12	0.84	
2BB	1.053/324	4.6 ± 1.0		$93 \pm 8/242 \pm 9$			8.40	0.79/0.67	$N_{\rm H} > N_{\rm gal}$
2BB	1.096/325	2.7[f]		$110 \pm 6/253 \pm 10$			8.48	0.58/0.59	
BB × edge	1.486/324	0.5 ± 0.3		201 ± 3	0.66^{+12}_{-17}	0.67 ± 0.08	8.30	1.02	
BB – gauss	1.631/324	0.5 ± 0.3		196 ± 3	0.76 ± 0.02	0.1[f]	8.23	0.97	EW = −83 eV
2BB × edge	1.051/323	2.7[f]		$123 \pm 11/254 \pm 15$	0.63 ± 0.03	0.26 ± 0.11	8.47	0.61/0.58	
2BB – gauss	1.015/322	2.7[f]		$140 \pm 14/283 \pm 30$	0.66 ± 0.05	0.13 ± 0.05	8.51	0.82/0.41	EW = −79 eV
NSA	1.347/326	1.8 ± 0.4		98 ± 3			8.37	1.65	
2NSA	1.042/324	6.7 ± 1.3		$27^{+6}_{-2}/118^{+7}_{-10}$			8.47	1.38/3.00	$N_{\rm H} > N_{\rm gal}$
2NSA	1.156/325	2.7[f]		$67^{+7}_{-12}/150^{+12}_{-20}$			8.56	0.76/1.16	
NSA × edge	1.079/324	2.6 ± 0.5		97 ± 3	0.65 ± 0.02	0.40 ± 0.08	8.43	1.92	
NSA + gauss	1.304/325	1.5 ± 0.4		101^{+4}_{-2}	0.53[f]	0.0[f]	8.40	1.59	EW = 12 eV
2NSA × edge	1.053/323	2.7[f]		$82^{+15}_{-17}/154^{+200}_{-40}$	0.64 ± 0.03	0.31 ± 0.09	8.53	0.46/1.45	

[a] BB and NSA temperatures are evaluated at infinity and at the NS surface, respectively. It is $T_{\infty} = T/(1+z)$; see text for details.
[b] Observed flux in the 0.2–10 keV band derived from the EPIC pn spectrum of the first observation.
[c] Bolometric flux for the thermal components (NSA and BB) derived from the EPIC pn spectrum of observation 0601180101.
[d] No error estimate due to bad fit.
[e] $N_{\rm gal} = 2.65 \times 10^{20}\,\rm cm^2$ (Kalberla et al. 2005).
[f] Parameter fixed in the fit.

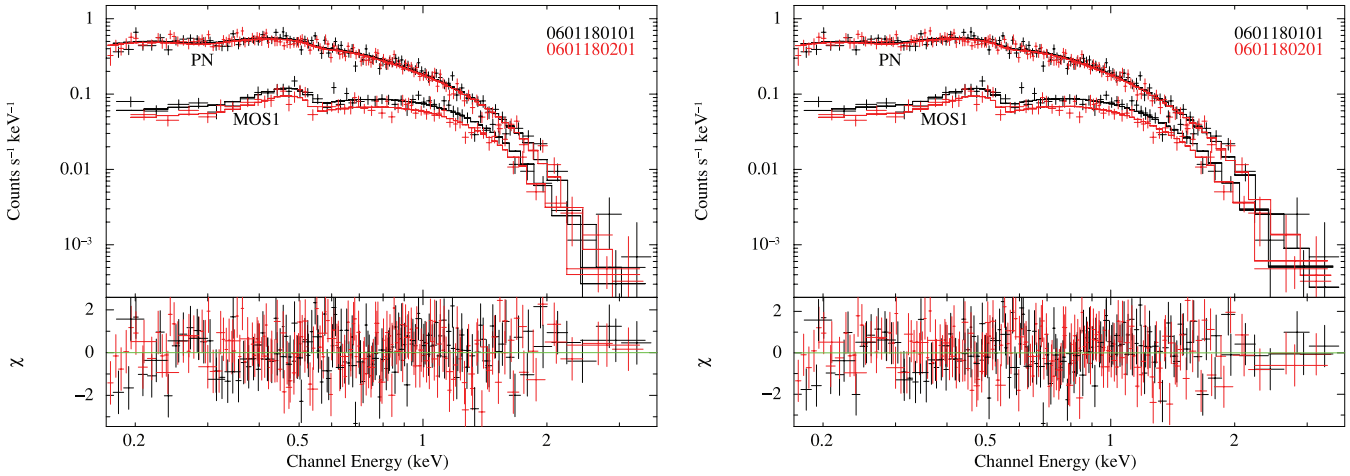

Figure 2. Left panel: EPIC pn and MOS1 spectra fitted with a double BB model. Right-hand panel: EPIC pn and MOS1 spectra modelled with a double NSA model. Both figures show best-fitting models in which the value of $N_{\rm H}$ has been left free. See Table 2 and text for details.

give a larger value, which may suggest the presence of a local absorption component. However, fixing the $N_{\rm H}$ at the Galactic value does not deteriorate the fits considerably (see, again, Table 2). Data and best-fitting models based on two thermal components (BB+BB and NSA+NSA with free $N_{\rm H}$) are shown in Fig. 2. Unfortunately, based on present spectral data only, it is not possible to discriminate between a picture in which the spectrum originates from two zones of the NS surface (with temperatures at infinity of ∼80 and 250 eV if the emission is modelled with blackbodies, or ∼55 and 150 eV if NSA models are used), and one in which the star surface is at uniform temperature (of $T_\infty \sim 80$ eV, NSA) with an absorption edge at ∼0.65 keV present in the spectrum (for a discussion about the possible discrimination based on other arguments, see Section 6.1).

We notice that, in the BB+BB and NSA+NSA models, the contributions of the two thermal components cross near ∼0.65 keV, which is probably the reason why the spectral fit can be accommodated by introducing a feature around this energy. This is at odds with Shevchuk et al. (2009), who proposed as a best-fitting model a NSA plus emission line: including a Gaussian emission line in the NSA model (with an energy fixed at 0.53 keV, the value derived by Shevchuk et al. 2009) improves the fit only slightly (see Table 2) and the line equivalent width (EW) of 12 eV is smaller than that derived from the *Chandra* spectrum (28 eV). Instead, we found that the fit improves by including an additional feature in absorption (the energy resolution is not sufficient to differentiate between an absorption edge and a negative Gaussian profile). Furthermore, we also found that both models based on two thermal components seem to further improve by introducing an absorption feature (either, edge or Gaussian line) at ∼0.65 keV. For instance, by adding an absorption edge to the BB+BB model (with fixed $N_{\rm H}$) gives an F-test statistic value of 7.94, and chance probability of 4×10^{-4}.[3]

Finally, we tested a 2BB+PL model. The reason for this is that there are some data points in the pn spectrum above 3 keV, although they have low significance (the background dominates at these energies, and they could also be caused by improper background subtraction). The PL photon index was fixed at 2. We found that the PL contribution to the total flux is ∼8 per cent. Again, the fit results in an increased $N_{\rm H}$ as compared to the 2BB case. We conclude that the existence of a PL non-thermal component up to a flux level of about 10 per cent cannot be excluded. In order to have further insights on this issue, spectra with better S/N above 3 keV are needed.

3.4 *XMM–Newton* timing analysis

Given the rather different observing modes and sampling time among the three instruments (Δt of ∼5.67 ms, 1.75 ms and 2.6 s for pn, MOS2 and MOS1, respectively) we first used all the event lists extracted from the three instruments during the two observations together, and assumed the largest (MOS1) sampling time in order to look for signals with periods larger than 5.2 s. Moreover, in order to maximize the sensitivity of the coherent pulsation search we minimize to two (one for each observation) the number of averaged power spectra. Significant power spectrum peaks were searched for by using the algorithm described in Israel & Stella (1996). No significant peak (above a 3.5σ confidence threshold on 2.097.152 frequency trials) has been found. The corresponding 3σ upper limit on the pulsed fraction (defined as the semi-amplitude of modulation divided by the mean source count rate) is about 10 per cent in the 5.2–10^3 s range (consistent, although tighter, with the constraints set by Shevchuk et al. 2009).

The signal search was then carried out by using the pn and MOS2 event lists only and with a time resolution of 5.67 ms in order to sample periods as short as ∼12 ms. A highly significant peak (∼11.5σ; see Fig. 3) was found at a frequency of 16.89242(2) Hz, corresponding to a period of 59.19816(7) ms (uncertainties refer to the intrinsic Fourier resolution of the power spectrum in Fig. 3). Such a short and strictly coherent period could be only accounted for by the spin period of a rotating NS.

A more accurate determination of the period, for each XMM observation, can be obtained by fitting the phases of the modulation over different time intervals. However, we noticed that the simultaneous MOS2 and pn light curves folded to the above period show a phase shift of about 0.10 and 0.15 (for the first and second observation, respectively), making any results inferred from the phase fitting analysis unreliable. The presence of both phase shift and

[3] We warn that, although widely used, the F-test is not strictly speaking a suitable method to test the significativity of (narrow) spectral lines and edges. These numbers must therefore be treated as an indication only. Given the uncertainties in modelling the continuum, further assessment of the significance of the feature (e.g. through Monte Carlo simulations) is not warranted.

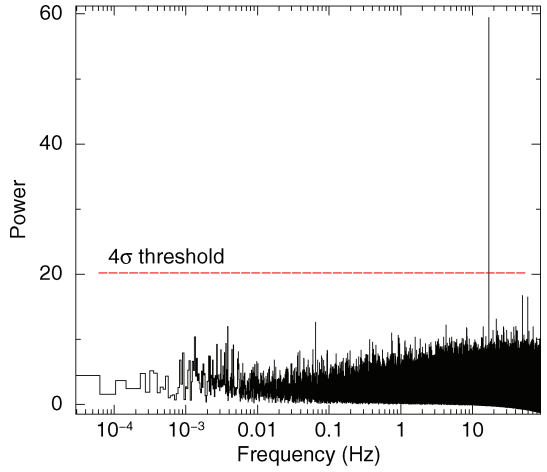

Figure 3. EPIC pn and MOS2 power spectrum together with the 4σ detection threshold (dashed line). The power peak corresponding to the $\sim$59 ms signal is evident.

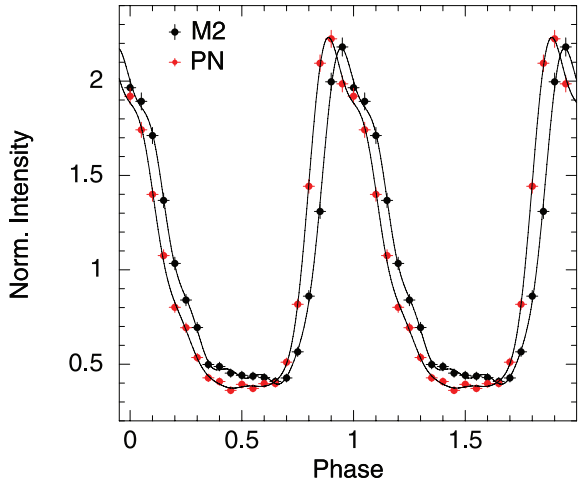

Figure 4. EPIC pn and MOS2 (M2) background-subtracted light curves of PSR B1509−58 folded at the best inferred period of $\sim$150 ms. The solid lines represent the best fit obtained by adopting a model with a sinusoidal plus four harmonics.

pulse distortion between MOS and pn was also detected in other relatively fast pulsars, such as PSR B1706−44 (with a pulse period of 102 ms; McGowan et al. 2004). In order to further check for the presence of the observed phase shift we also analysed the data from another pulsar, namely PSR B1509−58 (pulse period of $\sim$150 ms), observed by *XMM–Newton* in 2000 September with the pn and MOS2 in the same observational modes also set for our observations. The pn and MOS2 folded light curves of PSR B1509−58 are reported in Fig. 4. The phase shift is statistically significant and equal to 0.050 ± 0.001, corresponding to 7.5 ± 0.2 ms. Therefore, in the following we decide to use only the pn data given that no calibration to assess the absolute timing accuracy of the MOS exists (see the latest *XMM–Newton* EPIC technical reports[4]), and because of the pn larger statistics.

[4] http://xmm2.esac.esa.int/docs/documents/CAL-TN-0018.pdf and http://www2.le.ac.uk/departments/physics/research/src/Missions/xmm-newton/technical/mallorca-2008-04/08_04_09_mallorca_mos_timode_mgfk.pdf

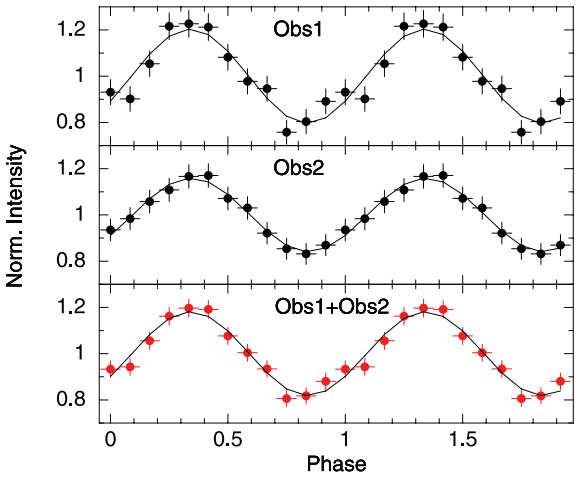

Figure 5. EPIC pn background-subtracted light curves folded at the best periods (see text for details) for the first *XMM–Newton* observation (upper panel, obs. ID: 0601180101), the second observation (middle panel, obs. ID: 0601180201) and the whole data set together (lower panel).

In order to obtain a refined value of the period we divided the first pn observation (obs. ID: 0601180101) in four time intervals of duration $\sim$5000 s and inferred the phase of the modulation in each interval (see Dall'Osso et al. 2003, for more details). The scatter of the phase residuals was consistent with a strictly periodic modulation at the best period of $P = 59.19821(1)$ ms or $\nu = 16.892404(5)$ Hz (90 per cent confidence, 55094 MJD). Unfortunately, the inferred accuracy is not enough to keep the phase coherency between the two observations which are separated by about 40 d (the inferred period uncertainty of the first *XMM–Newton* observation translates to a time uncertainty, at the epoch of the second pointing, of $\sim$220 ms corresponding to almost four period cycles). Correspondingly, we inferred a period separately for the pn data set of the second observation (obs. ID: 0601180201) resulting in a best value of $P = 59.19822(1)$ ms or $\nu = 16.892399(4)$ Hz (90 per cent confidence), consistent with the period of the observation 0601180101. The corresponding 3σ upper limit on the first period derivative $\dot{P}$ is $<9 \times 10^{-15}$ s s^{-1}.

No significant variations have been detected between the two observations (see Fig. 5). The signal shape is almost sinusoidal with pulsed fractions of 18 ± 3 per cent [90 per cent confidence, defined as $(C_{\rm max} - C_{\rm min})/(C_{\rm max} + C_{\rm min})$, where $C_{\rm max}$, $C_{\rm min}$ are the maximum and minimum number of counts]. The upper limit on the presence of a second harmonic is of the order of 5–7 per cent (3σ confidence level).

Finally, we searched for pulsation in the *Chandra*/HRC-I archive data (obs. ID: 8508) with the aim of obtaining another period measurement and therefore a measure of the $\dot{P}$ or a more constraining upper limit on it. No coherent signal was found, and the corresponding 3σ upper limit on the pulsed fraction is larger than 100 per cent.

3.5 Gamma-ray data analysis and results

Gamma-ray observations could represent an important step to unveil the nature of Calvera. In particular, the detection of pulsed emission at gamma-ray energies can in principle be useful to constrain the period derivative (and then the rotational energy loss rate) thanks to the large data spans typically provided by the current generation of

gamma-ray telescopes with time tagging accuracy as low as a few μs.

Hence, we searched for possible gamma-ray counterparts of Calvera in the catalogue of gamma-ray sources (Abdo et al. 2010b) detected by the LAT pair-production detector on board the *Fermi* Gamma-ray Space telescope (Atwood et al. 2009), and in the AGILE gamma-ray bright source catalogue (Pittori et al. 2010). No entries (spatial detections) in the gamma-ray catalogues are compatible with the X-ray source position within 3σ errors.

Nevertheless, it was worth performing a timing analysis on the LAT data, since the search for source timing signatures can be more sensitive than the spatial analysis to detect and evaluate the flux of weak periodic sources (see e.g. the case of PSR B1509−58; Abdo et al. 2010c), though typically giving higher statistical errors on the flux. In order to perform gamma-ray timing analysis we retrieved the available LAT public data on Calvera (photon data and spacecraft data) through the *Fermi* Science Support Center (FSSC) web data-server interface.[5] We analysed LAT data collected from 2008 August 4 (beginning of science phase) to 2010 April 27 (LAT runs 239557417 through 294038606, where the numbers refer to the Mission Elapsed Time (MET) in seconds since 00:00 UTC in 2001 January 1). During most of this time *Fermi* was operated in sky scanning survey mode (viewing direction rocking 35° north and south of the zenith on alternate orbits).

We performed LAT standard data processing using GTSELECT, GTMKTIME and GTBARY tools obtained from the HEADAS distribution of the *Fermi* ScienceTools (version v9r15p2) built on Scientific Linux 5 64 bit operating system. We selected $E > 100$ MeV events extracted within the 'region of interest' (ROI) of 2 degrees from X-ray source position (S/N ratio of *Fermi*-LAT pulsars is typically maximized taking ROI of ∼1°–2° around pulsar position; Abdo et al. 2010a). We selected only events with high probability of being photons ('diffuse' event class = 3, data quality = 1) collected within 105° maximum zenith angle (applying ROI-based zenith angle cut) and excluding data acquired during passages through the South Atlantic Anomaly. Solar system ephemeris JPL DE405 were used for the barycentric corrections. With the above selections, we obtained 2518 counts for the whole ∼1.8 yr data span.

The search for the Calvera timing signature in gamma-ray started from the ephemeris provided by the X-ray observations (ν and upper limit on $|\dot{\nu}|$). Standard epoch folding was performed within 10σ errors from the X-ray ephemeris. A grid of gamma-ray frequencies and frequency derivatives was explored with steps oversampling by a factor of 10 the canonical resolution allowed by the data span, $\nu_{\rm res} = 1/T_{\rm span} = 2 \times 10^{-8}$ Hz and $\dot{\nu}_{\rm res} = 2/T^2_{\rm span} = 7 \times 10^{-16}$ Hz^2, where $T_{\rm span}$ is the time-span of the data. Pearson's χ^2 statistics was applied to the 10-bin folded pulse profile resulting from each period search trial. Bin-independent parameter-free Z^2_n-test statistics (Buccheri et al. 1983) was also applied to the data.

A significant pulsed signal from Calvera was detected by both χ^2-test and Z^2_n-test ($\nu = 16.892401975(2)$ Hz, $\dot{\nu} = -1.2(7) \times 10^{-16}$ Hz^2, $P = 0.059198212396(7)$ s, $\dot{P} = 4(2) \times 10^{-19}$ s s^{-1}, Z^2_n-test = 26.2, $\sigma = 4.7$ with $n = 1$ harmonics). A reference epoch of 55094 MJD is assumed for the gamma-ray timing analysis. Weighting the corresponding detection probabilities with the number of independent ν and $\dot{\nu}$ trials ($n_{\rm trials} \sim 100$) the overall gamma-ray pulse significance is $\sim 3.7\sigma$, corresponding to a fake detection probability of only 3×10^{-4}. We verified that our analysis procedure does not produce fake detections even considering ν and $\dot{\nu}$ ranges much larger ($n_{\rm trials} > 10^4$) than those compatible with the X-rays ephemeris. In obtaining our timing solutions, the position of the source was held at the *Chandra* coordinates reported in Section 3.1. We have checked that the positional uncertainty ($\leq$1 arcsec) does not significantly affect barycentric corrections and then the rotational parameters resulting from our timing analysis.

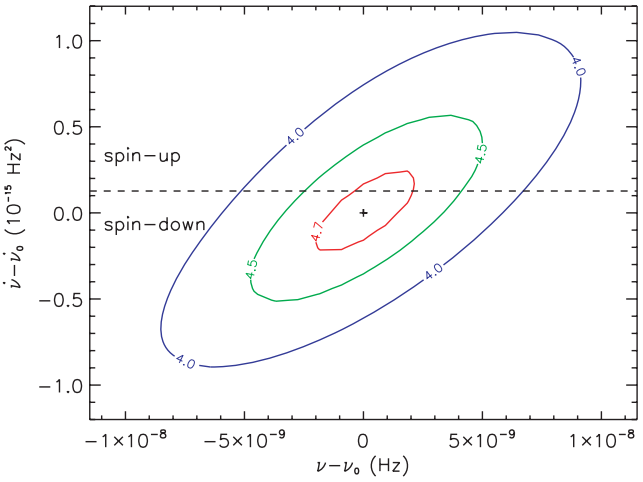

Figure 6. The $\nu - \dot{\nu}$ contour plot for the gamma-ray timing solutions with Z-test significance >4 sigma. The most significant detection is $\nu_0 = 16.892\,401\,975(2)$ Hz, $\dot{\nu}_0 = -1.2(7) \times 10^{-16}$ Hz^2 (timing epoch 55094 MJD). The horizontal dashed line corresponds to $\dot{\nu} = 0$. See text for details.

Fig. 6 shows the $\nu - \dot{\nu}$ contour plot related to the gamma-ray timing solutions with Z-test significance >4 sigma. Due to $\nu - \dot{\nu}$ timing solution degeneracy, as it is evident from the plot, positive frequency derivatives cannot be in principle excluded although unlikely (we also note that the deep optical limit allows to rule out accretion from a binary companion) and only upper limits on $|\dot{\nu}| < 10^{-15}$ Hz^2 ($|\dot{P}| < 5 \times 10^{-18}$ s s^{-1}) can be conservatively claimed. In case of spin-down, this corresponds to a rotational energy loss $\dot{E}_{\rm rot} < 10^{33}$ erg s^{-1}. If the spin-down is caused by magneto-dipolar braking the upper limit on the magnetic field is $B < 5 \times 10^{10}$ G.

Obviously, tight constraints on the ephemeris will rely on longer data spans. In particular, $>4\sigma$ S/N on the $\dot{\nu}$ measurements is expected from 1 year of further *Fermi*-LAT observations.

The energy-resolved gamma-ray light curves related to the most significant solution (corresponding to the cross in Fig. 6) are shown in Fig. 7. A single broad peak is detected in the gamma-ray light curves without significant pulse shape variations as a function of energy.

The pulsed flux was computed considering all the counts above the minimum of the light curve, using the expression PF = $(C_{\rm tot} - nN_{\rm min})/{\rm Exp} \equiv C_{\rm pul}/{\rm Exp}$, where $C_{\rm tot}$ is the total number of counts, n is the number of bins in the light curve, $N_{\rm min}$ are the counts of bin corresponding to the minimum and Exp is the exposure in cm^2 s units. This method is 'bin dependent', but we have checked that different (reasonable) choices of both the number of bins (i.e. $n > 10$) and the location of the bin centre (10 trial values were explored) do not significantly affect the results. The pulsed counts for $E >$100 MeV are $C_{\rm pul} = 455 \pm 95$ count ($C_{\rm pul} = 275 \pm 75$ for $E >$300 MeV) corresponding to ∼15 per cent of total gamma-ray counts (the unpulsed flux can be ascribed to diffuse gamma-ray background emission). Comparable results are obtained using the expression adopted for the calculation of the X-ray pulsed fraction

[5] http://fermi.gsfc.nasa.gov/ssc/.

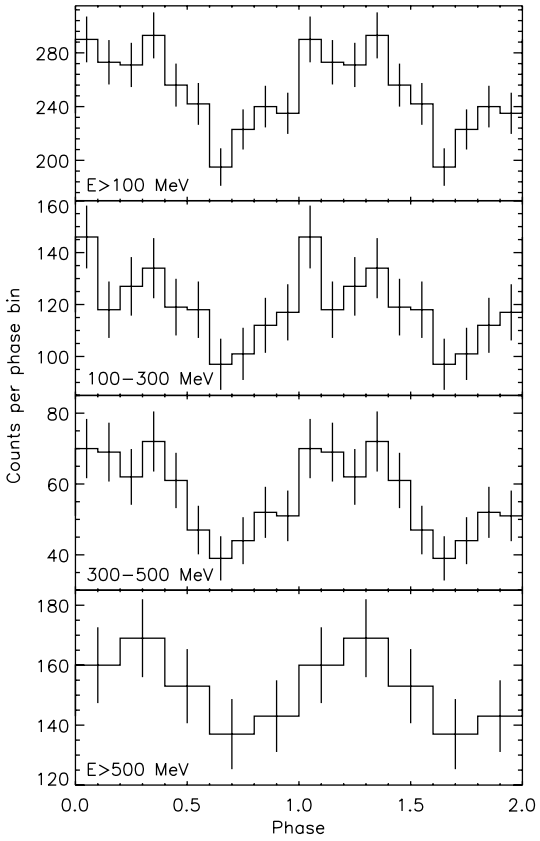

Figure 7. Energy-resolved gamma-ray light curves (total counts) taken with *Fermi*-LAT. The pulsed signal is detected at $\sim 5\sigma$ in the whole $E > 100$ MeV band ($\sim$6 ms bin resolution). Gamma-ray emission from Calvera seems present at least up to $\sim$1 GeV though the pulsed signal significance is low at $E > 500$ MeV.

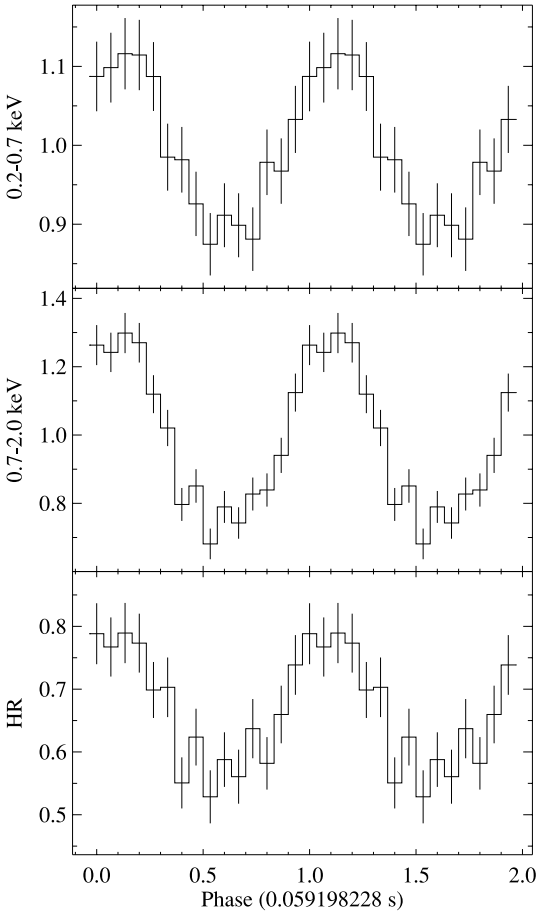

Figure 8. Background-subtracted folded light curves obtained from the combined EPIC pn data of both observations in two different energy bands. The pulse profiles are normalized by the corresponding average count rates of 0.197 count s^{-1} and 0.133 count s^{-1} (0.2–0.7 keV and 0.7–2.0 keV, respectively). The bottom panel shows the hardness ratio HR = CR(0.7 − 2.0 keV)/CR(0.2 − 0.7 keV), where *CR* denotes the count rate in the corresponding energy band.

$(C_{\max} - C_{\min})/(C_{\max} + C_{\min})$. No pulsed signal can be significantly ($>3\sigma$) disentangled when data are restricted to narrower ranges in the low energy part (e.g. 100–300 MeV), although a modulation (in phase with the profiles obtained from broader energy bands) is still visible in the light curves (Fig. 7). Therefore, only rough gamma-ray spectral measurements can be performed with the present count statistics.

We made a LAT exposure cube from the spacecraft data file using GTLTCUBE procedure from *Fermi* ScienceTools and created the exposure map using the GTEXPCUBE tool. The resulting total exposure of the whole data span at the source position for $E > 100$ MeV is 2.2×10^{10} cm^2 s (5.4×10^{10} cm^2 s for $E > 300$ MeV), corresponding to a $E > 100$ MeV pulsed flux PF $= (4.1 \pm 0.9) \times 10^{-8}$ ph cm^{-2} s^{-1} [PF $= (6.4 \pm 1.7) \times 10^{-9}$ ph cm^{-2} s^{-1} for $E > 300$ MeV]. We corrected the pulsed flux accounting for the additional source counts falling outside the ROI (2° radius) estimated according to the instrument point spread function (PSF). We also verified that the pulsed fraction systematic errors due to spectral uncertainties in the exposure calculation are below count statistics errors. A comparison of $E > 100$ MeV and $E > 300$ MeV pulsed fluxes provides a rough gamma-ray photon index estimate $\alpha = 2.5 \pm 0.5$ (100 MeV–10 GeV).

In the frame of a spin-powered pulsar interpretation, the resulting $E > 100$ MeV luminosity, assuming a beaming angle of 1 sr, is $L_\gamma = 1.3 \times 10^{32} d_{\rm kpc}^2$ erg s^{-1}, where $d_{\rm kpc}$ is the source distance in kpc. The observed gamma-ray luminosity and the upper limit on the spin-down power ($<10^{33}$ erg s^{-1}) constrain the distance below $\sim$1 kpc, considering a likely gamma-ray conversion efficiency upper limit of 10 per cent.[6]

3.6 *XMM–Newton* pulse phase spectroscopy

In order to look for spectral variations in the X-ray flux of Calvera we first created background-subtracted light curves in the energy bands 0.2–0.7 keV and 0.7–2.0 keV and a hardness ratio by dividing the count rates in the hard band by those in the soft band. We used single- and double-pixel events (PATTERN = 0–4) from the EPIC pn data, combining both observations and extracted events from the same source and background regions as used for the extraction of the spectra. The light curves were folded with a period of 59.198228 ms, derived from a simple chi-square folding test of the data, assuming a constant period. The resulting pulse profiles and the hardness ratio as function of pulse period are shown in Fig. 8.

[6] An efficiency of $\sim$10 per cent is indeed very high, although it may be attained in some sources. As an example, Mignani, Pavlov & Kargaltsev (2010) recently revised the distance of PSR 1055−52, finding a relatively low value of $\sim$300 pc. This gives a gamma-ray efficiency as high as 10 per cent, in line with the value assumed in this paper.

Table 3. Pulse phase spectroscopy.

Model	χ^2/d.o.f.	$N_{\rm H}$	Low-temperature BB component			High-temperature BB component		
			kT_1	$F_{\rm bol}^{\rm max}$	$F_{\rm bol}^{\rm min}$	kT_2	$F_{\rm bol}^{\rm max}$	$F_{\rm bol}^{\rm min}$
		10^{20}		10^{-13}	10^{-13}		10^{-13}	10^{-13}
		($\rm cm^{-2}$)	(eV)	(erg $\rm cm^{-2}\,s^{-1}$)	(erg $\rm cm^{-2}\,s^{-1}$)	(eV)	(erg $\rm cm^{-2}\,s^{-1}$)	(erg $\rm cm^{-2}\,s^{-1}$)
PPS1	1.17/242	4.2 ± 1.0	96 ± 10	8.15	6.32	246 ± 13	7.37	5.71
PPS2	1.01/241	4.3 ± 0.7	96 ± 10	7.54	7.42	246 ± 12	8.04	5.06

Bolometric fluxes for the BB components derived from the EPIC pn spectrum of observation 0601180101.

We then investigated the possibility of a changing relative contribution of the two spectral components with spin phase. To this aim, we have produced EPIC pn spectra (MOS1 has insufficient time resolution for pulse phase spectroscopy, PPS) around pulse maximum and minimum (each covering 0.5 in phase) and fitted the four spectra (two observations, two phases) with the double BB model. Similarly to the case of the pulse average spectra, we fitted all the pn spectra simultaneously. We performed fits with two model flavours: models PPS1 and PPS2. In model PPS1 only the relative overall normalizations are allowed to vary between spectra. This corresponds to a case without variation in spectral shape between the two phase intervals. In PPS2 we allow different normalizations for all the BB components, i.e. a variation of the relative contribution of the two BB components is possible. The derived spectral parameters and bolometric fluxes are summarized in Table 3, while spectra are shown in Fig. 9. Again, because of no significant long-term flux variations, we only report in the table the fluxes inferred from the pn spectra from the first observation (obs. ID: 0601180101).

Both models assume no temperature changes with pulse phase, and provide a fully acceptable fit. Given the current statistics, we are not in the position to allow more free parameters in the fit or to test different spectral models. As one can see from Table 3, model PPS2 yields a better description of the spectral behaviour with pulse phase (F-test statistic value of 41.3 and chance probability 6.9×10^{-10}). This shows that the spectral shape changes with pulse phase, as also indicated by the variations in the hardness ratio (Fig. 8), and suggests that the relative contribution of the hotter component is higher during pulse maximum and lower during minimum.

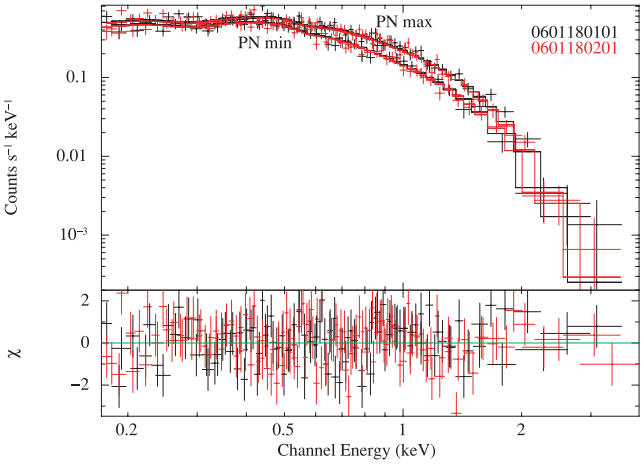

Figure 9. EPIC pn spectra from two different pulse phase intervals covering pulse maximum and minimum from the two *XMM–Newton* observations. The histograms show the double BB model PPS2 as described in the text and Table 3.

4 RADIO OBSERVATIONS

Following the discovery of pulsations in the X-rays and gamma-rays, the X-ray position of Calvera was searched for radio pulsations using the Effelsberg telescope with the aim of better understanding the nature of the source and, in particular, in case of detection, to measure the period derivative given the higher precision generally achievable in the radio band. Observations were taken on MJD 55330 at 1.36 GHz with a bandwidth of 240 MHz spread over 410 frequency channels using a sample time of 55 μs for 78 min and for four epochs (a total of 312 min). On MJD 55337 a further observation was taken using the same setup for 60 min.

These observations were folded using the X-ray ephemeris and searched over a range of frequency-dependent time delays to correct for the unknown amount of dispersion (caused by free electrons along the line-of-sight) between Calvera and the Earth. These dispersion measures ranged from 0 to 1000 $\rm cm^{-3}$ pc and the step size was optimized for a pulsar with a period of ∼60 ms. The observations were also searched blindly for any periodicities and for single dispersed pulses (though impulsive radio frequency interferences at Effelsberg make this latter type of search very difficult).

No radio pulses from Calvera were detected down to a sensitivity of $S = 0.05$ mJy for each of the observations assuming a duty cycle of 5 per cent. These observations improved the previous flux density upper limit (obtained by Hessels et al. 2007, with the Westerbork Synthesis Radio Telescope) of almost an order of magnitude (by assuming a spectral index of 1.7; see Kramer et al. 1998). Assuming a distance $d < 1$ kpc, this translates into an upper limit of 0.05 mJy $\rm kpc^2$ for the pseudo-luminosity (defined as $S \times d^2$) at 20 cm, a limit that encompasses 99 per cent of all known pulsars (and 100 per cent of the mildly recycled ones to which Calvera could belong; see Section 6.2.2) reported in the version 1.40 of the Australia Telescope National Facility (ATNF) Pulsar Catalogue.[7]

Note that the Effelsberg observations are only sensitive to pulsations and not to continuum emission; inspection of archival NRAO/VLA Sky Survey (NVSS) data (Condon et al. 1998) showed no clear evidence of point-like or extended radio sources in the vicinity of Calvera (see Section 5).

5 SEARCH FOR DIFFUSE EMISSION IN THE FIELD OF CALVERA

In order to search for possible sources of diffuse emission in the proximity of Calvera, we analysed in detail the *XMM–Newton* and *ROSAT* all-sky survey (RASS) images.

Using *XMM–Newton* MOS1 and MOS2 data, we created colour images for the second *XMM–Newton* observation. At low energies, different features are clearly visible. North of Calvera we can see an

[7] http://www.atnf.csiro.au/research/pulsar/psrcat/

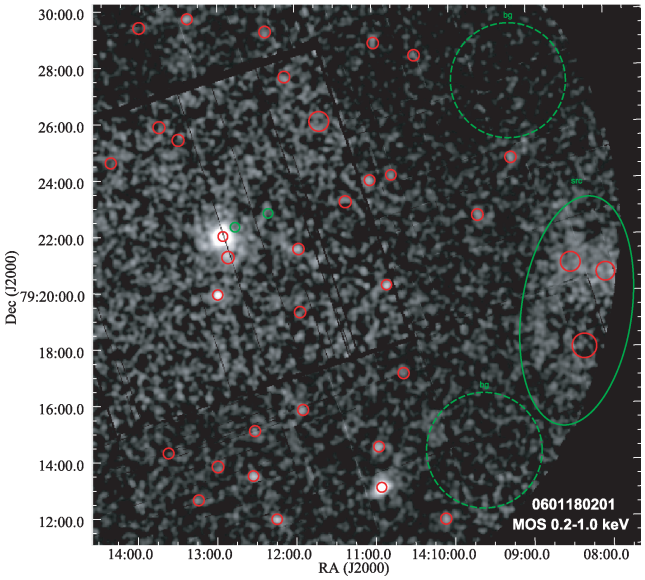

Figure 10. MOS1+MOS2 image in the 0.2–1.0 keV band. The spectrum of the extended source west of Calvera has been extracted from the region inside the green ellipse. The two green dashed circles indicate the regions used to extract the background spectrum. Small green and red circles are as in Fig. 1 (right-hand panel).

area with increased soft emission, which, however, shows a sharp edge at the border of the CCD, and therefore it is likely to be related to higher noise in one of the MOS CCDs. More interestingly, the image shows an extended region of soft X-ray emission west of Calvera (at the outer rim of the field of view, where the source detection software also identifies three sources; see the combined MOS 0.2–1.0 keV image shown in Fig. 10). The extended emission is relatively soft and best visible below 1.0 keV.

The extended emission is also clearly seen in the standard RASS images, where it is best visible in the 0.1–0.4 keV band, but also seen in the 0.5–2.0 keV band. The *ROSAT* source detection also located a source within the extended emission region: this detection is included in the bright source catalogue (Voges et al. 1999), but lacks an optical identification (Zickgraf et al. 2003). The *ROSAT* images do not show significant emission north of Calvera, confirming that the feature seen in the EPIC image is likely to be due to CCD noise.

Although it is unlikely that the extended emission is related to Calvera, considering their angular separation of 13 arcmin, it remains an interesting detection. Its X-ray morphology is reminiscent of an old SNR, or a pulsar wind nebula. Further insights on its nature can be obtained by a spectral analysis. Therefore, we extracted the MOS1+MOS2 spectra from an elliptical region (246 and 117 arcsec semi-axes) covering the extended source. The background was extracted using two circular regions (122 arcsec radius), free of *XMM–Newton* detections (see Fig. 10). Spectra were fitted using a non-equilibrium ionization (NEI) model (Fig. 11), which reproduces the X-ray spectra of faint SNRs, e.g. in the Magellanic Clouds (see e.g. Filipovic et al. 2008). We found that the spectrum of the diffuse emission is well represented by this model ($\chi^2_r = 1.35$ for 46 d.o.f.), and clearly shows the (unresolved) emission line triplets of O VII and N VI. From the fit, O appears to be overabundant by a factor of ∼2–3. Unfortunately, due to the scarce data, the temperature is unconstrained (it has been fixed at 0.7 keV during the fit) and we could only derive an upper limit on the column density, $N_{\rm H} < 1.5 \times 10^{20}\,{\rm cm}^{-2}$ (3σ).

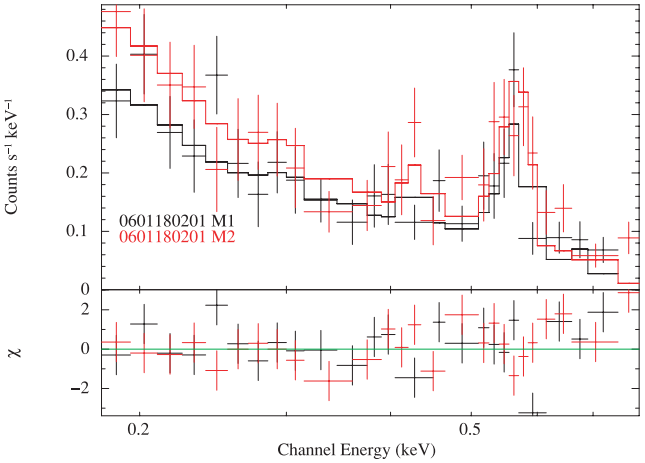

Figure 11. Spectral fit of MOS1/MOS2 data from the extended emission with a NEI model (see text for details).

In order to investigate further the nature of the extended emission, we inspected the DSS R, B and IR images, but did not find evidence for spatial structures. We also checked for evidence of diffuse Hα emission at the position of the *XMM–Newton* extended source using images from The Virginia Tech Spectral-Line Survey (VTSS),[8] which has pixel size of 1.6 arcmin and field of view of $10^\circ \times 10^\circ$ per pointing. Unfortunately, the Calvera field is not yet available in the processed survey data. No other Hα survey data are available, which cover the field with a sufficient spatial resolution.

We then inspected the field in radio continuum using data from the NRAO/NVSS at a frequency of 1.4 GHz, which covers the sky at $\delta > -40^\circ$ with beams of 45 arcsec full width at half-maximum (FWHM) (Condon et al. 1998). From the NVSS data (Fig. 12) we could not find evidence for any radio source, either point-like or extended, at the position of Calvera, down to a flux level of ∼0.1 mJy (3σ) at 1.4 GHz. As far as the radio emission from Calvera itself is concerned, this upper limit is much less constraining than those discussed in Section 4. The closest radio source detected in the NVSS data is located at ∼30 arcsec from the position of Calvera, it is not extended and has an estimated flux of ∼0.47 mJy. At the same time, we found about a dozen radio sources (∼0.5–2.5 mJy) within a circle of 5 arcmin radius centred on the position of the X-ray extended emission. However, none of them shows evidence of extended radio emission on angular scales larger than ∼2.5 arcmin. We could not find evidence of diffuse emission over the whole searched area down to a limit of ≈1.5 μJ arcsec^{-2}, which we assume as the upper limit on the radio brightness of the extended emission detected in the *XMM–Newton* and *ROSAT* data.

6 DISCUSSION

We have presented a new multi-wavelength study of the NS candidate Calvera (1RXS J141256.0+792204), based on two new *XMM–Newton* observations, on one set of publicly available *Fermi*-LAT data and on one new observation taken at Effelsberg in the radio band. We also used *Chandra* and *ROSAT* archival data. We discussed previous determinations of the source position, and concluded that at present the best estimate is that based on absolute *Chandra* ACIS-S astrometry, i.e. $\alpha = 14^{\rm h}12^{\rm m}55\overset{\rm s}{.}84$, $\delta = +79^\circ22'03\overset{''}{.}7$ with a 90 per cent confidence error of 0.6 arcsec.

[8] http://www.phys.vt.edu/ halpha/

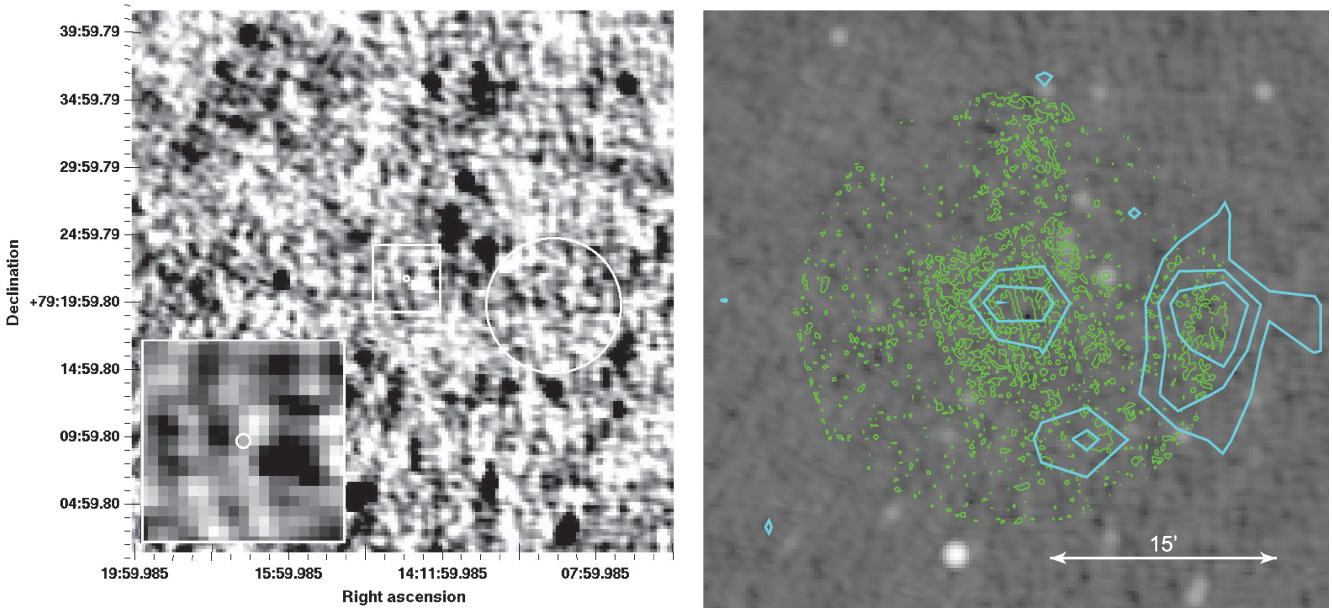

Figure 12. Left-hand panel: NVSS image of the Calvera field. The contrast has been increased to show faint sources. The position of Calvera is marked by the white circle whose radius has been fixed to 10 arcsec for a better visualization. The closest radio source is detected ∼30 arcsec north-west of the Calvera position and is well away from the *Chandra* error circle. The white square (5×5 arcmin^2) marks the region highlighted in the inset (lower-left corner). The large white circle (5 arcmin radius) is drawn around the position of the extended source seen in the *XMM–Newton* and *ROSAT* data. No extended radio emission is detected on angular scales larger than ∼2.5 arcmin down to a flux limit of $\approx$1.5 μJ arcsec^{-2}. Right-hand panel: same as in the left-hand panel, with the X-ray contours from *XMM–Newton* (green) and RASS (cyan) overplotted. For *XMM–Newton* we used the combined MOS 0.2–1.0 keV image (just one contour level is shown, corresponding to 5.4×10^{-3} count s^{-1} arcmin^{-2}) and for RASS the total 0.1–2.4 keV image [three contour levels: (2.8, 4.1 and 5.5) $\times$ 10^{-3} count s^{-1} arcmin^{-2}].

The combination of *XMM–Newton* and *Fermi*-LAT has allowed us to discover the period of the source, $P \simeq 59.19$ ms, and to place an upper limit on its spin-down rate, $|\dot{P}| < 5 \times 10^{-18}$ s s^{-1}. We warn that positive frequency derivatives cannot be excluded, although, based on the contours presented in Fig. 6, they appear to be less likely. This possibility will be addressed by future timing monitoring, and will not be discussed further hereafter. Instead, in case of spin-down our measurements correspond to a rotational energy loss $\dot{E}_{\rm rot} < 10^{33}$ erg s^{-1}, a large characteristic age >1.55 Gyr and a low magnetic field, $B < 5 \times 10^{10}$ G (under the assumption of magneto-dipolar breaking).

Although the best fit of the X-ray spectrum is not unique (see Table 2), according to our findings (see Section 6.1 for a detailed discussion), the most likely spectral model consists of two thermal components (blackbodies) with temperatures $kT_1 \sim 150$ eV, $kT_2 \sim 250$ eV, plus possibly an absorption edge at ∼0.65 eV [$\sim 0.65(1+z)$ eV when measured at the star surface]. Similar spectral features are found in other classes of thermally emitting NS, as the XDINSs (see e.g. Turolla 2009, and references therein) or 1E 1207.4−5209 (e.g. Bignami et al. 2003; Mori & Hailey 2006), which, however, are characterized by a much larger spin period. By interpreting the edge as an electron or a proton cyclotron feature gives $B = 6 \times 10^{10}(1+z)$ G or $B = 6 \times 10^{13}(1+z)$ G, respectively: the former value is not too different from the limit inferred from the timing (which, however, only constrains the large-scale dipolar component). Instead, we do not find substantial evidence for the emission line at ∼0.5–0.6 keV proposed by Shevchuk et al. (2009); on the other hand, considering the thermal character of the underlying continuum, a feature in absorption appears a more likely outcome. The X-ray luminosity is $L_{\rm X} \sim 10^{32} d_{\rm kpc}^2$ erg s^{-1}(with small variations depending on the assumed spectral model; see Table 2), and there is no evidence for a PL tail up to a flux contribution of ∼10 per cent.

Overall, Calvera is a very puzzling pulsar. It has a thermal soft X-ray spectrum (with a possible absorption feature), but, at variance with other similar sources as the XDINSs, it is not a 'soft' source: through our timing search we found that it is still detected at $>4\sigma$ even at $E > 300$ MeV. A rough estimate of the 100 MeV–10 GeV photon index gives $\alpha = 2.5 \pm 0.5$. The gamma-ray luminosity is $L_\gamma = 1.3 \times 10^{32} d_{\rm kpc}^2$ erg s^{-1}, computed by assuming a beaming angle of 1 sr. Assuming a gamma-ray conversion efficiency upper limit <10 per cent, and assuming that the observed gamma-ray luminosity is powered by spin-down, the upper limit on the rotational energy loss ($<10^{33}$ erg s^{-1}) provides a quite strong constraint on the distance, that turns out to be below ∼1 kpc (much lower distances might result from the future estimate of the true value of $\dot{E}_{\rm rot}$).

The source is not detected in the optical and radio bands. Based on the non-detection of the source on a *Gemini*-North+GMOS imaging of the field, Rutledge et al. (2008) reported a 3σ upper limit of $g > 26.3$ mag, or $F_g < 0.11$ μJy, at 4750 A. As for the radio band, our Effelsberg observation allowed us to set a deep upper limit on the source-pulsed emission of 0.05 mJy, assuming a duty cycle of 5 per cent.

Finally, we report evidence for diffuse X-ray emission in the field of Calvera, ∼13 arcmin west of the source.

In the following, we will first discuss the spectral and timing results, and then we will elaborate on the implications of our new findings regarding the perspectives on the source interpretation.

6.1 The new timing and multi-wavelength spectral properties

Thanks to the high sensitivity of *XMM–Newton* at low energies, we have been able to reach a good characterization of the X-ray spectrum. In agreement with previous findings based on *Chandra* data (Shevchuk et al. 2009), we found that the X-ray spectrum cannot

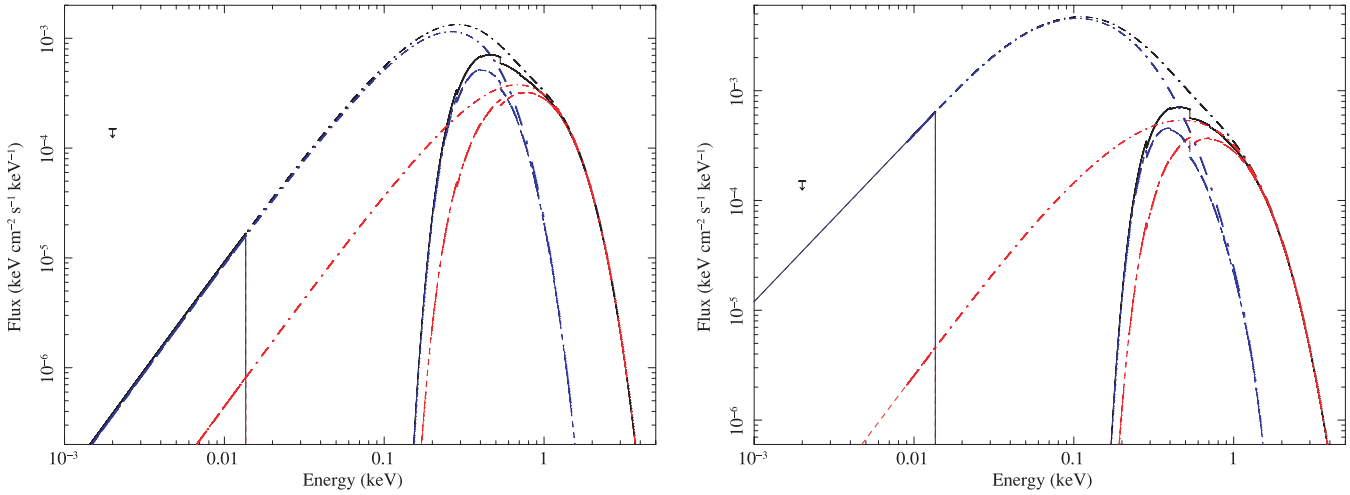

Figure 13. Left panel: the best-fitting double BB model shown in Fig. 2 (left-hand panel) extrapolated in the optical band. Red lines: hot component, blue lines: cold component, black lines: total. Solid and dash–dotted lines correspond to absorbed and unabsorbed spectra. The arrow marks the *g*-band upper limit inferred from *Gemini*-North+GMOS imaging (see text and Rutledge et al. 2008). Right-hand panel: same as in the left-hand panel for the NSA+NSA model shown in the right-hand panel of Fig. 2.

be reproduced by a single-component model, while a satisfactory fit can be obtained by adding a spectral feature to an atmospheric model (NSA). This spectral decomposition has the advantage that it requires a relatively low value of interstellar absorption ($N_{\rm H} \approx 2.6 \times 10^{20}$ cm^2), compatible with that inferred from H I maps in the source direction (Kalberla et al. 2005; Shevchuk et al. 2009). In this case, the star surface emits at a uniform temperature of ≈100 eV, and the feature is more likely to be an absorption edge at ≈0.65(1 + *z*) keV.

The main problem with a scenario based on uniform surface emission is that our measurement of a relatively large X-ray pulsed flux (PF ∼ 18 per cent) seems to rule out a relatively smooth thermal map. Pulse profiles produced by the thermal surface distribution induced by a simple core-centred dipolar magnetic field have been investigated long ago by Page (1995), under the assumption that the surface emits (isotropic) BB radiation. Because of gravitational effects and of the smooth temperature distribution (the temperature monotonically decreases from the poles to the equator), the pulse modulation is quite modest (PF $\lesssim$ 10 per cent).

Indeed, our spectral fits show that the spectral decomposition is not unique: an equally likely possibility is that the spectrum is made of two thermal components (again with possibly a spectral feature at ∼0.6–0.7 keV), reflecting the presence of two zones of the NS surface at different temperatures. The two components can be modelled with either a NSA or a BB, with the difference that, since atmospheric models are harder than a BB at the same temperature, the temperatures inferred from a NSA+NSA fit are systematically lower than those obtained from a double BB model. As a consequence, a BB+BB and a NSA+NSA decomposition result in very different predictions for the amount of flux expected in the optical band (see e.g. Fig. 13), and in principle it may be possible to use optical observations to discriminate between the two options (see e.g. Pavlov et al. 1996). Unfortunately, in practice, this is unfeasible. The *g*-band upper limit from the *Gemini*-North+GMOS imaging translates into ≈1.5×10^{-4} keV cm^{-2} s^{-1} keV^{-1} at ≈2×10^{-3} keV, which is still compatible even with the large fluxes expected in the atmospheric emission scenario (see Fig. 13, right-hand panel). In order to use this approach to robustly discriminate among X-ray spectral models, we would need an upper limit on the optical flux at least 1–2 orders of magnitude lower, which requires deep imaging of the field down to $g \sim 29$–31. This is clearly unfeasible with the current instrumentations.

In this respect, some insights may be obtained exploiting the detection of the source at high energy based on the LAT timing analysis. In fact, the fits to X-ray data with two thermal components using a NSA+NSA or a BB+BB model result in different estimates of the distance and of the size of the emitting regions (see Table 4). In Table 4, we report the predicted distances inferred by the fits based on a double NSA model, for the limit case of the colder component emitted from the whole NS surface. This is an overestimate for the area of the colder region, since a second, hotter NSA component is present. However, the ratio of the cold/hot areas is ≈0.02–0.05 (similar to that implied by the BB+BB fit), and our estimates of the distance would not change significantly by assuming that ∼95 per cent (instead of 100 per cent) of the whole surface is emitting at the lowest temperature. In this case, if $N_{\rm H}$ is fixed at a value compatible with the Galactic absorption, the distance turns out to be quite large, ∼1.5–2 kpc, which seems too large when compared with the limit

Table 4. Radii of the emitting regions and source distance inferred from the spectral modelling with two thermal components. In the case of the BB+BB fit, the reported values for the radius of the hot and cold component correspond to a source distance of 1 kpc; for smaller distances they should be scaled down accordingly. In the case of the NSA+NSA models, the source distance is computed by assuming that the colder component is emitted by the whole star surface, and using $R_{\rm star} = 12$ km and $M_{\rm star} = 1.4\,{\rm M}_\odot$. We warn that, in this case, the inferred distances depend on the assumed values, although slightly. For instance, would the mass be as large as $2\,{\rm M}_\odot$, the distance will turn out to be a factor of ∼15–17 per cent smaller. The interstellar absorption is left free to vary during the fit or fixed at the Galactic value; values are reported in Table 2.

Model	$N_{\rm H}$	$R_{\rm cold}/R_{\rm hot}$ (km)	Distance (pc)	Comment
BB + BB	Free	3.1/0.43		$N_{\rm H} > N_{\rm gal}$
BB + BB	Fixed	1.9/0.36		
(BB + BB)×edge	Fixed	1.6/0.36		
NSA + NSA	Free		175	$N_{\rm H} > N_{\rm gal}$
NSA + NSA	Fixed		1550	
(NSA + NSA)×edge	Fixed		2250	

inferred from the gamma-rays (unless the gamma-ray conversion efficiency is extremely high). Similarly, the BB+BB model is only compatible with emission from the whole surface (from the coldest component) if the star is at 5 kpc or more, which, again, contradicts the gamma-ray limit.

In fact, a BB+BB model is compatible with the relatively large PF only for a $d \sim 1$ kpc, which gives quite small BB radii ($\sim$0.5–3 km) suggesting a scenario in which the two thermal components originate in two different small spots at the star surface. If this is the case, the rather small emitting areas, together with a pulsed fraction of $\sim$18 per cent, and the sinusoidal pulse shape, are suggestive of a geometry in which the star is a quite aligned rotator seen at a large inclination angle. This is also supported by the pulse-phase spectroscopy and hardness ratio variation, which indicate that there is only a moderate spectral evolution with phase. This may be explained if both emitting caps are always (partially) in view as the star rotates, with the hotter spot becoming more visible near the pulse maximum. The gamma-ray pulses are also quite sinusoidal, with no evidence for changes at different energies and a pulsed fraction similar to that in the X-rays. However, the current impossibility of phase-align the X- and gamma-ray observations (see Section 3.4 for all details) prevents to reach any conclusions on the relative positions of pulse maxima.

6.2 The nature of the source

Our new findings, in particular the new discovery of the X-ray and gamma-ray period and the measurement of an upper limit for the spin-down rate, unequivocally identify Calvera as a relatively fast spinning NS, and provide long-sought crucial information to shed light on to the conundrum about its nature (see below and Section 2).

Based on the preliminary spectral information available at that time, Rutledge et al. (2008) attempted to classify Calvera by comparing it with different classes of compact objects that occupy different regions in the luminosity/effective temperature/emitting radius spaces. In light of the new discovery of a relatively fast period, some of the previously proposed scenarios as that of an XDINS or a magnetar are now ruled out. Similarly, Calvera's spin period is too large to be compatible with an interpretation in terms of a (fully) recycled millisecond pulsar.

In the context of the $P - \dot{P}$ diagram, Calvera appears as one of the transition objects that populate the zone between the bulk of the pulsar crowd and the group of recycled millisecond pulsars (in the bottom-left corner of Fig. 14). Also, the rotational parameters (hence the values of $\dot{E}$ and B) are consistent with those of the CCOs, the most similar of which is the source in Kesteven 79.

These findings, taken together with the fact that the source is apparently isolated and it is not associated with a SNR (but see Section 6.2.1), open exciting novel possibilities, among which the most likely are that of an 'orphan CCO' or that of a mildly recycled source that was once a member of a high-mass binary system (see Sections 6.2.1 and 6.2.2).

6.2.1 A new CCO?

Based on the timing properties and on the thermal character of the spectrum, a first possibility is that Calvera is a new CCO. In this respect, we note that the X-ray energetics of the source is also unusual. The upper limit on $\dot{E}_{\rm rot}$ ($<10^{33}$ erg s^{-1}) is only a factor of 10 larger than the X-ray luminosity inferred from *XMM–Newton* data ($\sim 10^{32}$ erg s^{-1} at 1 kpc). While an efficiency of $\sim$10 per cent in gamma-ray is not unusual (see Section 3.5), the conversion efficiency in the X-ray band is typically lower, of the order of $\sim 10^{-2}$ to 10^{-3} or less (Kargaltsev & Pavlov 2008; Becker, Huang & Prinz 2010). If the X-ray emission is powered by the source spin-down (e.g. in the case in which it originates from two hot spots at the star surface, heated by back-flowing magnetospheric currents), a similar efficiency would imply a very low distance, of the order of $\sim$100–300 pc (or even less, considering that our estimate of the upper limit on $\dot{E}_{\rm rot}$ is conservative). Alternatively, the thermal X-ray emission may have a different origin (e.g. anisotropic surface cooling). In this case we note that, based on our spectral fitting, we cannot exclude that a $\sim$10 per cent of the X-ray flux is ascribed to a non-thermal PL component; if this fraction of the total X-ray emission is spin-down powered, an efficiency of 10^{-2} translates in $d \sim 1000$ pc.

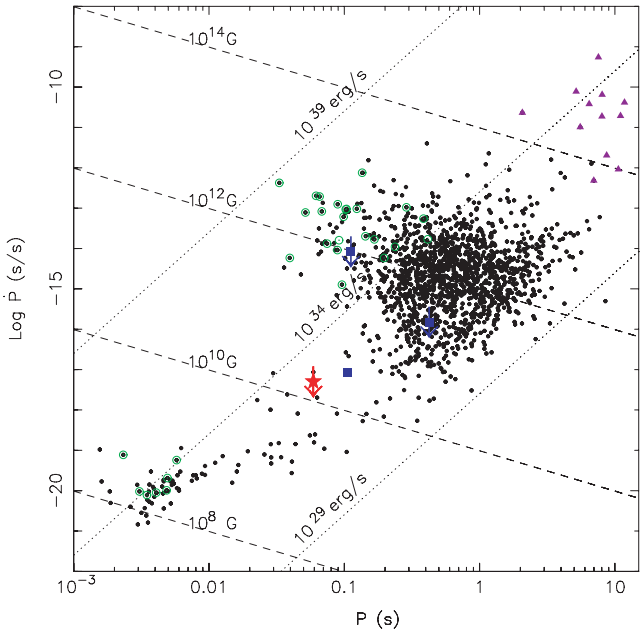

Figure 14. $P - \dot{P}$ diagram for Galactic field NSs: the red star marks our upper limit for Calvera, black dots are radio pulsars (from the ATNF pulsar catalogue; Manchester et al. 2005), the blue squares are CCOs with a measured (or an upper limit value of) $\dot{P}$ (Gotthelf & Halpern 2007, 2009; Halpern & Gotthelf 2010) and violet triangles are magnetars (data from Mereghetti, 2008). The NSs encircled in green are sources detected by *Fermi* (Abdo et al. 2010a). Dashed lines indicate equal magnetic field, while dotted lines indicate equal value for the rotational energy losses, $\dot{E}_{\rm rot}$.

Interestingly, apart from binary systems and magnetar sources, that are thought to be powered, respectively, by accretion or by the super-strong magnetic field, the only sources that may be characterized by $\dot{E}_{\rm rot} \lesssim L_{\rm X}$ are the (slowly rotating) XDINSs (Kaplan & van Kerkwijk 2009) and the CCOs. For instance, the only CCO for which the spin period derivative has been (recently) measured (i.e. PSR J1852+0040 in Kesteven 79, see Halpern & Gotthelf 2010) has $L_{\rm X} \sim 10\dot{E}_{\rm rot}$. In all other cases, only an upper limit on the period derivative is available; still, 1E 1207.4−5209 has $L_{\rm X} \sim 2 \times 10^{33}$ erg s^{-1} and $\dot{E}_{\rm rot} < 10^{32}$ erg s^{-1} (Gotthelf & Halpern 2007). Puppis A has $\dot{E}_{\rm rot} < 10^{33}$ erg s^{-1}, that does not exclude an efficiency of $\sim 10^{-2}$ (Gotthelf & Halpern 2009). The X-ray emission of CCOs is thermal and characterized by a double BB spectrum, without the presence of hard X-ray tail, similar to the X-ray spectrum Calvera.

A possible counter-argument for the CCO interpretation might be raised by comparing with figs 2–3 of Rutledge et al. (2008): Calvera's surface temperature is quite low with respect to those

typically observed in this class, and, since the typical X-ray luminosity of other CCOs is $\sim 10^{33}$ erg s^{-1}, this interpretation would require a source distance of 2–3 kpc (against the constraint from the gamma-rays). Nevertheless, we warn that these problems with a CCO interpretation may not be too severe. The comparison of Calvera with CCOs based on the temperature comes with caveats, since it does not account for the fact that different CCOs might have different ages, or that the thermal history of a CCO might have been modified by a recent phase of accretion. Also, we note that the derived CCO luminosities are based on the estimated distances of the host SNRs, which are usually affected by uncertainties of the order of 50 per cent or more. Thus, using CCO luminosities as standard candles could be risky.

The possible association with a SNR, or lack thereof, is a crucial piece of information to determine whether Calvera is, or not, a CCO. We already noticed that the extended X-ray source detected west of Calvera in the *XMM–Newton* and *ROSAT* data shows evidence for triplets of O VII and N VI in the spectrum, which are robust signatures of SNRs (although a final confirmation could only come from Hα/S II/O III ratios). If we assume that Calvera has moved 13 arcmin away from the centre of this putative SNR, the kinematic age of Calvera (and in turn the age of the SNR) results in $t = 39000 d_{\rm kpc}/v_{100}$ yr, where v_{100} is the source velocity in units of 100 km s^{-1}. This is much lower than the 1.55 Gyr age estimated from the spin parameters. However, this is a common characteristic of CCOs: the lower limits on their spin-down ages (although smaller than that of Calvera) are always much larger than the SNR ages. A way out, within the 'anti-magnetar' interpretation (Halpern & Gotthelf 2010), is to assume that the initial spin periods of these pulsars were very close to their current values, so that they have not changed much during the pulsar's lifetime. In other words, the spin-down age is not representative of the true age of the source but only reflects its initial conditions at birth.

Despite these considerations, we consider it unlikely that this extended emission is associated with Calvera. At a distance of $\sim$1 kpc a typical CCO-associated SNR is expected to be much larger: for instance the 7 kyr old SNR associated with 1E 1207.4−5209 would appear with an angular size of $\sim 2^\circ/d_{\rm kpc}$. Instead, the size of the extended emission derived from the *ROSAT* contours is 16×8.5 arcmin^2, which suggests that the SNR is a background object. We note that the upper limit on the column density inferred from the SNR spectrum ($N_{\rm H} < 1.5 \times 10^{20}$ cm^{-2}) is smaller than the Galactic $N_{\rm H}$ in the direction of Calvera. This would make the extended emission likely closer; however this comparison is hampered by the limited photon statistics of the diffuse source. Considering the angular separation and the low $\dot{E}_{\rm rot}$ of the pulsar, it is also unlikely that the extended source is a pulsar wind nebula associated with Calvera.

On the other hand, if Calvera is an underluminous CCO at a low distance of only $\sim$300 pc, the large spatial scale would make it hard to detect the SNR with narrow field X-ray instruments like EPIC. Furthermore, it cannot be ruled out that Calvera is an old ($\geq$1 Myr) CCO and that its host SNR has already expanded and faded away in the interstellar medium.

This 'orphan CCO' scenario is potentially intriguing, especially in view of the possible connections between old CCOs and other NS classes. Still, in this scenario Calvera would be a quite extreme case. So far, no CCO has been detected at gamma-ray energies. This may be due to observational limits: first, in cases in which the embedding SNR dominates it is difficult to resolve the gamma-ray emission from the CCO. Secondly, detecting CCOs as weak gamma-ray pulsars is difficult because only three of these sources

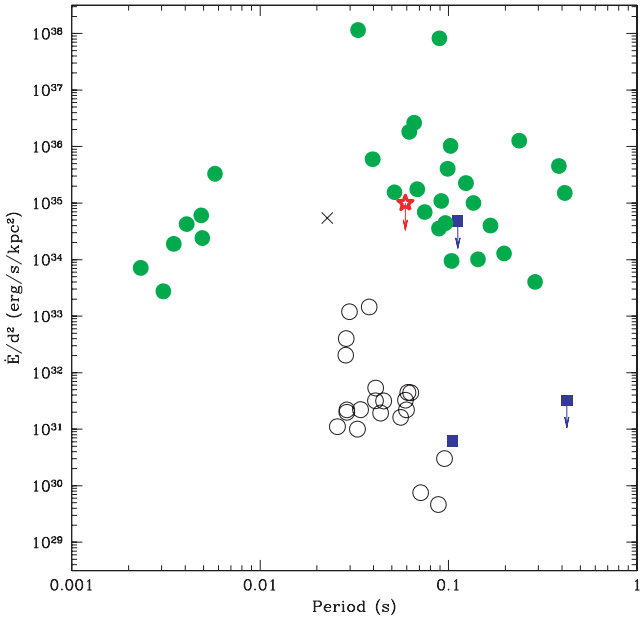

Figure 15. Ratio $\dot{E}_{\rm rot}/d^2$ plotted versus spin period for various samples of NSs. The green filled dots represent all the pulsars detected so far in gamma-rays by *Fermi*-LAT (according to Abdo et al. 2010a). The black empty dots represent all the radio pulsars in the ATNF pulsar catalogue having spin period between 20 and 100 ms and surface magnetic field smaller than 10^{11} G (i.e. those generally interpreted to be mildly recycled pulsars; none of them has been detected so far by *Fermi*-LAT in gamma-rays). The red star represents the position of Calvera, based on our upper limit on $\dot{E}_{\rm rot}$ and on a (low) distance of 100 pc. The blue filled squares refer to the three CCOs with a known value (or an upper limit) for the spin period derivative and hence for $\dot{E}_{\rm rot}$. The black cross reports the position of the mildly recycled pulsar in the Double Pulsar binary PSR J0737−3039, for which there is a tentative detection (to be confirmed) of pulsed emission in gamma-ray with *Agile-GRID* (Pellizzoni, in preparation), and no published detection with *Fermi*-LAT. All the distances in this plot (but for the three CCOs) have been derived from the best-estimate reported in the ATNF pulsar catalogue at 2010 June 30 (Manchester et al. 2005). In most cases, they are inferred from the dispersion measure of the radio pulsar.

have an X-ray period and only one (Kes 79) has a measured $\dot{P}$. In Fig. 15 we report the ratio $\dot{E}_{\rm rot}/d^2$ (an often-used figure of merit for the detectability in the gamma-ray band of a source with $\dot{E}_{\rm rot} < 10^{34}$ erg s^{-1}; e.g. Abdo et al. 2010a) plotted against the spin period for various relevant samples of NSs (see the caption of Fig. 15). As we can see, among the CCOs with a measured (or an upper limit value of) $\dot{P}$, two of them have a relatively low value of $\dot{E}_{\rm rot}/d^2$, which may hamper the gamma-ray detection. Would a CCO nature be confirmed, Calvera will represent a unique case and our timing technique, here applied to *Fermi* data, constitutes a key tool to investigate the high-energy spectrum of other members of the class (the most promising candidate for this search being Puppis A, whose upper limit for $\dot{E}_{\rm rot}/d^2$ is, as in the case of Calvera, compatible with a relatively large value).

6.2.2 Is Calvera the first discovered mildly recycled gamma-ray pulsar?

The spin period and the upper limit on the spin period derivative place Calvera well within the area of the P–$\dot{P}$ diagram which is known to be populated by the so-called mildly recycled radio pulsars. Hence, the plausible and very intriguing possibility that

Calvera represents the first case ever of a mildly recycled gamma-ray pulsar.

It is commonly believed that recycled radio pulsars are formed when a relatively old NS is spun up by accretion while in a binary system (Bisnovatyi-Kogan & Komberg 1974). The amount of mass accreted, hence of spin-up, is related to the duration of the X-ray binary phase, and ultimately depends on the mass of the companion: low-mass X-ray binaries are thought to be the progenitors of the so-called 'fully' recycled radio pulsars (often referred to as millisecond radio pulsars[9]) with spin periods of a few ms, while binary systems with an intermediate- or a high-mass companion give rise to mildly recycled radio pulsars with periods of tens of ms (e.g. Lorimer et al. 2004).

In this picture, we note that the lack of detection of Calvera in the radio band (down to a very deep flux density limit) can be plausibly explained by the relatively narrow radio beam missing the Earth. As to the X-ray luminosity, one can apply similar considerations to those reported for the CCO hypothesis (see Section 6.2.1), i.e. a rotation-powered nature requires a distance as low as $\sim$100–300 pc. The double BB X-ray spectrum, however, is somehow unusual for a recycled pulsar, since most of them are characterized by either single-component (either BB or PL) or BB+PL spectra.

The observability in the gamma-ray band is an unprecedented feature for NSs with the rotational parameters of Calvera and one may wonder if it is due to some peculiar emission process operating in this source or to observational biases. In this respect we first note that, provided the distance is around or below 300 pc, the gamma-ray efficiency nicely fits with the average value (around a few per cent) seen in the gamma-ray pulsars observed by *Fermi*-LAT. Even assuming a larger distance of 1 kpc, the gamma-ray efficiency remains compatible with that observed in at least one other object (Mignani et al. 2010). Also, the gamma-ray spectrum is within the range of those shown by the *Fermi* pulsars, although pointing towards the tail of the steepest spectral indices in the spectral parameter distribution. By inspecting Fig. 15, we can see that the large majority of the NSs with rotational parameters in the range of those of the mildly recycled radio pulsars (empty dots in the diagram) have a $\dot{E}_{\rm rot}/d^2$ ratio well below the minimum value which resulted in a detection with *Fermi* so far (filled dots; Abdo et al. 2010a). Although the location of Calvera in this plot is highly unconstrained, we notice that in principle its $\dot{E}_{\rm rot}/d^2$ ratio can be at least $\sim$10 times larger (for a distance less than 300 pc) than that of the best cases among the mildly recycled radio pulsars (similar results hold when plotting the analogous parameter $\sqrt{\dot{E}_{\rm rot}}/d^2$; e.g. Abdo et al. 2010a). Therefore, in the framework of the interpretation of Calvera as a mildly recycled gamma-ray pulsar (for which a short distance is largely preferred), it seems that the relatively large observed gamma-ray flux of Calvera is due to its proximity rather than to a stronger intrinsic emission with respect to the other known rotation-powered NSs.

It is worth noting that the relatively steep gamma-ray spectral index of Calvera could be echoed in the spectrum of the mildly recycled pulsar in the Double Pulsar binary (PSR J0737−3039A; Burgay et al. 2003; Lyne et al. 2004). For the latter (whose $\dot{E}/d^2$ is also very promising; see Fig. 15) there is a tentative detection with *Agile-GRID* (Pellizzoni, in preparation) and no detection so far with *Fermi*-LAT, which would indicate a very soft gamma-ray spectrum (interestingly enough, also the X-ray spectrum of the Double Pulsar appears unusually soft among the recycled pulsars; Pellizzoni et al. 2008; Possenti et al. 2008). If confirmed by future analysis, this may be a peculiarity of the high-energy emission from the class of mildly recycled pulsars.

As to the evolution of Calvera, the presence of a main sequence, or a giant or a white dwarf companion can be ruled out by the deep optical upper limit. This in turn suggests that Calvera is not the descendant of an intermediate-mass X-ray binary, since the endproducts of these systems usually comprise a NS orbiting a heavy carbon–oxygen white dwarf or (in some peculiar cases; see e.g. Li 2002) a helium white dwarf. Given the above considerations, it seems very likely that Calvera was recycled in a high-mass X-ray binary, in which also the companion star eventually experienced a supernova explosion. The most probable outcome of this event is the disruption of the binary, with the release of two isolated NSs, one having the typical parameters of a ordinary pulsar and the other – usually dubbed disrupted recycled pulsar (DRP; i.e. see Lorimer et al. 2004) – having a moderate spin rate (in the range of few tens of ms) and a surface magnetic field which is intermediate between that of the ordinary pulsars and that of the fully recycled pulsars. Alternatively, there is the possibility that the binary system survives the supernova explosion, leading to the formation of a double neutron star (DNS) binary. If the absence of a binary companion will be supported by future dedicated campaigns of observation,[10] Calvera will enter the rare class of the DRPs, which would make its discovery particularly worthwhile for investigating various still open issues on the final stage of the evolution of high-mass X-ray binaries and on the supernova kick.

For instance, there is currently a large mismatch between the theoretical expectations on the relative number of DRPs and DNSs and the result of the observations. According to the fact that the survival of the binary in the second supernova explosion requires properly tuned parameters for the pre-supernova system and/or for the kick associated with the supernova event, population synthesis studies (e.g. Portegies-Zwart & Yungelson 1998) indicate that DRPs are expected to be generated at a significantly higher rate than DNSs. Since the rotational parameters of the NSs are similar in the two classes of objects, their lifetime in the radio band and their radio emission properties should also be similar and hence one would expect to detect up to $\sim$10 times more DRPs than DNSs (Lorimer et al. 2004). At variance with this prediction, to date eight DRPs in the Galactic field are reported, a number matching that of the eight known DNSs (from ATNF pulsar catalogue at 2010 June 30). Supernova kicks smaller than those usually assumed in population synthesis have been proposed to at least partially alleviate this problem: in fact that would reduce the gap between the birthrates of the DRPs and that of the DNSs.

Notably, the distances (derived from the dispersion measure) of the known DRPs (all selected in the radio band) cluster mostly between 2 and 3 kpc, with the closest source (PSR J2235+1506) located at 1.2 kpc. Therefore, Calvera would turn out to be much closer than all the other DRPs, suggesting the existence of a significant (if not even dominant) contribution of the gamma-ray pulsars to the population of the mildly recycled NSs. Were this the case, the

[9] By comparing again with figs 2–3 of Rutledge et al. (2008), we can see that, in principle, if the source distance were low ($\sim$ a few hundreds of pc), the properties of Calvera inferred from the BB+BB fit (i.e. typical temperatures around 100–200 eV and rescaled BB radii of $\sim$0.1–0.2 km) might be compatible with those of the fully recycled radio pulsars observed in 47 Tucanae. However, the now measured spin period rules out the millisecond radio pulsar scenario proposed by Rutledge et al. (2008).

[10] Our present data do not allow us a search for orbital periodicities.

current observed ratio between the number of radio-selected DRPs and DNSs could not be representative of the whole population. Of course, additional discoveries of mildly recycled gamma-ray pulsars (with particular emphasis for blind searches), as well as detailed binary pulsar population synthesis models are necessary to assess the biases due to the small-number statistics and to properly test the aforementioned hypothesis. The confirmation of a DRP interpretation for Calvera and the discovery of similar sources would have strong implications: e.g. it will impact the estimates of the beaming factor [i.e. the fraction of sky swept by the emission beam(s)] in the radio and gamma bands for the mildly recycled NSs, thus constraining their emission models; it will lead to increase in the overall birthrate of the descendants from high-mass X-ray binaries in the Galaxy; it will also suggest the existence of some DNS binary at close distance from the Earth and which escaped radio detection so far. This may in turn lead to an upward revision on the expected rate of events of merging of DNSs in the Galaxy, a key prediction for the current generation of ground-based gravitational wave detectors.

Once the spin-down rate (and hence the surface magnetic field) of Calvera will be measured it might be possible to estimate its initial spin period (post spin-up phase; see fig. 2 in Lorimer et al. 2004), as well as the time since the occurrence of the second supernova explosion in the progenitor binary. With the present data we can only notice that, in both the DRP and DNS hypotheses, Calvera is expected to be much younger than the age inferred from the spin-down rate (Arzoumanian, Corder & Wasserman 1999; Lorimer et al. 2004): e.g. for our upper limit on $\dot{P}$, the time elapsed from the second supernova would be 10^8 yr, under the hypothesis that Calvera was spun up by accretion of mass at the Eddington rate up to the limit imposed by its magnetic field (Lorimer et al. 2004). Since the position of Calvera – slightly outside the Galactic disc, at a distance of $<0.6 d_{\rm kpc}$ above the Galactic plane – could be ascribed to the kick imparted to the NS (or to the DNS binary) by the second supernova, a constraint on the time since the explosion (even better if complemented with constraints on the proper motion of the source) will in turn allow one to study the kick imparted to the NS (or to the DNS binary) in the supernova.

7 CONCLUSIONS

Thanks to our multi-wavelength campaign, we have been able to recognize in Calvera an intriguing, low magnetized pulsar with a relatively fast period, $\sim$59 ms. This rules out most of the previously proposed scenarios for the nature of the source. Calvera's properties are reminiscent of those of CCOs and mildly recycled pulsars, although other interpretations cannot be ruled out (mainly because our timing solution is still compatible with a spin-up scenario). On the other hand, even in comparison with the other members of these two classes, the source can be singled out thanks to its unique characteristics, mainly the hard gamma-ray emission joined to a thermal X-ray spectrum.

The discovery of peculiar, possibly transitional, sources such as Calvera is of the utmost importance to gain a full understanding of the Galactic NS phenomenology and to eventually establish links between the different classes into which isolated NSs have been catalogued up to now. The existence of bridging objects is progressively coming into view, as in the case of PSR B1509−58 for the magnetar/high-field spin-powered PSRs connection (Pellizzoni et al. 2009) of the newly discovered radio magnetar (Levin et al. 2010), or the bursting young pulsar PSR J1846−0258 (Gavriil et al. 2008). Furthermore, although Calvera is most likely to be isolated, the current optical limits do not allow us to exclude a NS companion, in which case the source would represent one of the rare DNS systems discovered in the Galaxy.

Given the unique placement of Calvera in this framework, further investigations aimed at better assessing its properties are definitely warranted. Accurate X-ray timing can provide a positive determination of the source spin-down rate, and a better characterization of its spectrum, especially concerning the presence of a high-energy PL tail and of spectral features, is bound to reveal much on the processes which power its X-ray emission, and ultimately on its true nature. Presently, we were able only to place an upper limit on the pulsed radio flux. Calvera may be genuinely radio quiet but the search for radio emission must be pursued further since a detection at radio wavelengths would yield an independent, accurate determination of $\dot{P}$, the dispersion measure and the star proper motion (the latter may also be pursed in the X-ray band; see Shevchuk et al. 2009). Follow-up X-ray and optical narrow-band imaging observations will allow one to better characterize the properties of the putative SNR, and to constrain both its age and its distance. All these issues are crucial to assess if there is indeed a connection between Calvera and the nearby diffuse emission, the presence of which was first reported in this investigation. New observations at gamma-ray energies will allow one to better constrain the source spin evolution, shed light on the spectral distribution at gamma-ray energies and how the latter changes with rotational phase. Finally, the search for gamma-ray emission from other sources with similar properties (CCOs, mildly recycled and low $\dot{E}_{\rm rot}$ PSRs, . . .) using the novel timing technique which led us to the detection of Calvera in the gamma-rays is certainly in order and will be the matter of future work.

ACKNOWLEDGMENTS

The work of GLI and RT is partially supported by INAF/ASI through grant AAE-I/088/06/0. PE acknowledges financial support from the Autonomous Region of Sardinia through a research grant under the program PO Sardegna FSE 2007–2013, L.R. 7/2007 'Promoting scientific research and innovation technology in Sardinia'. Based on observations obtained with *XMM–Newton*, an ESA science mission with instruments and contributions directly funded by ESAMember States and NASA. We acknowledge the *Fermi* Science Support Center at NASA/Goddard providing guest observers with smart public data retrieval services. The 100-m Effelsberg radio telescope is operated by the Max-Planck-Institut fuer Radioastronomie of the Max-Planck-Society. This research has made use of data obtained from the *Chandra* Data Archive and software provided by the *Chandra* X-ray Center (CXC) in the application package CIAO. We are grateful to an anonymous referee for several helpful comments.

REFERENCES

Abdo A. A. et al., 2010a, ApJS, 187, 460
Abdo A. A. et al., 2010b, ApJS, 188, 405
Abdo A. A. et al., 2010c, ApJ, 714, 927
Arzoumanian Z., Corder J. M., Wasserman I., 1999, ApJ, 568, 289
Atwood W. B. et al., 2009, ApJ, 697, 1071
Becker W., Huang H. H., Prinz T., 2010, ApJ, submitted (arXiv:1006.0335)
Bignami G. F., Caraveo P. A., De Luca A., Mereghetti S., 2003, Nat, 423, 725
Bisnovatyi-Kogan G. S., Komberg B. V., 1974, SvA, 18, 217
Buccheri L. et al., 1983, A&A, 128, 245
Burgay M. et al., 2003, Nat, 426, 531
Condon J. J., Cotton W. D., Greisen E. W., Yin Q. F., Perley R. A., Taylor G. B., Broderick J. J., 1998, AJ, 115, 1693

Dall'Osso S., Israel G. L., Stella L., Possenti A., Perozzi E., 2003, ApJ, 599, 485
De Luca A., 2008, in Bassa C., Wang Z., Cumming A., Kaspi V. M., eds, AIP Conf. Proc. Vol. 983, 40 Years of Pulsars: Millisecond Pulsars, Magnetars and More. Am. Inst. Phys., New York, p. 311
De Luca A., Caraveo P. A., Mereghetti S., Negroni M., Bignami G. F., 2005, ApJ, 623, 1051
Filipovic M. D. et al., 2008, A&A, 485, 63
Gavriil F. P., Gonzalez M. E., Gotthelf E. V., Kaspi V. M., Livingstone M. A., Woods P. M., 2008, Sci, 319, 1802
Gotthelf E. V., Halpern J. P., 2007, ApJ, 664, L35
Gotthelf E. V., Halpern J. P., 2009, ApJ, 695, L35
Gould A., 2003, AJ, 126, 472
Haberl F., 2007, Ap&SS, 308, 181
Halpern J. P., Gotthelf E. V., 2010, ApJ, 710, 941
Hessels J. W. T., Stappers B. W., Rutledge R. E., Fox D. B., Shevchuk A. H., 2007, A&A, 476, 331
Israel G. L., Stella L., 1996, ApJ, 468, 369
Kalberla P. M. W., Burton W. B., Hartmann Dap, Arnal E. M., Bajaja E., Morras R., Pöppel W. G. L., 2005, A&A, 440, 775
Kaplan D. L., van Kerkwijk M. H., 2009, ApJ, 705, 798
Kargaltsev O., Pavlov G. G., 2008, in AIP Conf. Proc. Vol. 983, 40 Years of Pulsars: Millisecond Pulsars, Magnetars and More. Am. Inst. Phys., New York, p. 171
Kramer M., Xilouris K. M., Lorimer D. R., Doroshenko O., Jessner A., Wielebinski R., Wolszczan A., Camilo F., 1998, ApJ, 501, 270
Lasker B. M. et al., 2008, AJ, 136, 735
Levin L. et al., 2010, ApJ, 721, L33
Li X. D., 2002, ApJ, 564, 930
Lorimer D. R. et al., 2004, MNRAS, 347, L21
Lyne A. G. et al., 2004, Sci, 303, 1153
Manchester R. N., Hobbs G. B., Teoh A., Hobbs M., 2005, AJ, 129, 1993
McGowan K. E., Zane S., Cropper M., Kennea J. A., Córdova F. A., Ho C., Sasseen T., Vestrand W. T., 2004, ApJ, 600, 343
McLaughlin M. et al., 2006, Nat, 439, 817
Mereghetti S., 2008, A&AR, 15, 225
Mignani R. P., Pavlov G. G., Kargaltsev O., 2010, ApJ, 720, 1635
Mirabel I. F., Dhawan V., Mignani R. P., Rodrigues I., Guglielmetti F., 2001, Nat, 413, 139
Monet D. G. et al., 2003, AJ, 125, 984
Mori K., Hailey C. J., 2006, ApJ, 648, 1139
Page D., 1995, ApJ, 442, 273
Page D., Lattimer J. M., Prakash M., Steiner A. W., 2004, ApJS, 155, 623
Pavlov G. G., Sanwal D., Teter M. A., 2004, in Camilo F., Gaensler B. M., eds, IAU Symp. 218, Young Neutron Stars and Their Environments. Astron. Soc. Pac., San Francisco, p. 239
Pavlov G. G., Zavlin V. E., Truemper J., Neuhaeuser R., 1996, ApJ, 472, L33
Pellizzoni A., Tiengo A., De Luca A., Esposito P., Mereghetti S., 2008, ApJ, 679, 664
Pellizzoni A. et al., 2009, ApJ, 695, L115
Pires A. M., Motch C., Turolla R., Treves A., Popov S. B., 2009, A&A, 498, 233
Pittori C. et al., 2009, A&A, 506, 1563
Portegies-Zwart S. F., Yungelson L. R., 1998, A&A, 332, 173
Possenti A., Rea N., McLaughlin M. A., Camilo F., Kramer M., Burgay M., Joshi B. C., Lyne A. G., 2008, ApJ, 680, 654
Roeser S., Demleitner M., Schilbach E., 2010, AJ, 139, 244
Rutledge R. E., Fox D. B., Shevchuk A. S. H., 2008, ApJ, 672, 1137
Shevchuk A. S. H., Fox D. B., Rutledge R. E., 2009, ApJ, 705, 391
Skrutskie M. F. et al., 2006, AJ, 131, 1163
Standish E. M., 2004, A&A, 417, 1165
Strüder L. et al., 2001, A&A, 365, L18
Turner M. J. L. et al., 2001, A&A, 365, L27
Turolla R., 2009, in Becker W., ed., Neutron Stars and Pulsars, Astrophysics and Space Science Library. Vol. 357, Springer, Berlin, p. 141
Voges W. et al., 1999, A&A, 349, 389
Wilms J., Allen A., McCray R., 2000, ApJ, 542, 914
Woods P. M., Thompson C., 2006, in Lewin W., van der Klis M., eds, Cambridge Astrophysics Series, Vol. 39, Compact Stellar X-ray Sources. Cambridge Univ. Press, Cambridge, p. 547
Zacharias N. et al., 2010, AJ, 139, 2184
Zavlin V. E., Pavlov G. G., Shibanov Y. A., 1996, A&A, 315, 141
Zickgraf F. J., Engels D., Hagen H. J., Reimers D., Voges W., 2003, A&A, 406, 535

This paper has been typeset from a TEX/LATEX file prepared by the author.